

Quasi non-universal shape exponents induced by step-droplets around (001) facet on the equilibrium crystal shape: The restricted solid-on-solid model with inter-step attraction of the point-contact type

Noriko Akutsu

Faculty of Engineering, Osaka Electro-Communication University,
Hatsu-cho, Neyagawa, Osaka 572-8530, Japan

E-mail: nori@phys.osakac.ac.jp

Abstract. The anisotropic surface free energy and the equilibrium crystal shape (ECS) $z = z(x, y)$ are calculated numerically by using the transfer matrix method with the product wave-function renormalization group (PWFRG) algorithm, which is a variant of the density matrix renormalization group method. The adopted surface model is the restricted solid-on-solid (RSOS) model having the inter-ledge attractions of the point-contact type (p-RSOS model). The surface gradient $\mathbf{p} = (\partial z / \partial x, \partial z / \partial y)$ is calculated by the PWFRG method as a function of the reduced coordinates $(X, Y) = (\eta_x / k_B T, \eta_y / k_B T)$, where $\boldsymbol{\eta}$ is the Andreev field to make surface be tilted. By analyzing the results, we obtain the first-order shape transition on the profile of the ECS, and the quasi non-universal shape exponents. For the vicinal surface tilted relative to (001) surface along $\langle 110 \rangle$ direction, the slope dependence of the mean step-height of the bunched steps $\langle n(\mathbf{p}) \rangle$ is calculated by Monte Carlo method. We derive the effective surface free energy which contains quadratic term with respect to $|\mathbf{p}|$ by taking into consideration the slope dependence of $\langle n(\mathbf{p}) \rangle$. The quasi non-universal shape exponents and other quantities obtained by the PWFRG calculations are reproduced thermodynamically from the effective surface free energy.

PACS numbers: 68.35.Md, 05.70.Np, 05.50.+q, 68.35.-p

1. Introduction

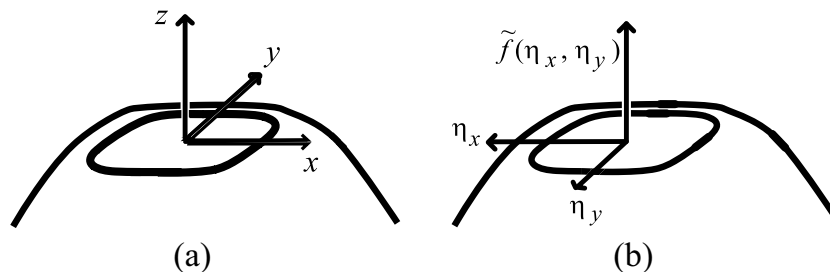


Figure 1. The schematic figure of the equilibrium crystal shape (ECS) and the Andreev free energy \tilde{f} (a) ECS $z = z(x, y)$. (b) The Andreev free energy as the function of the Andreev field (η_x, η_y) (Eq. (5) and Eq. (8)).

The step bunching has attracted attention from the view point of nanoscale technology, since novel self-organization techniques are expected by applying the self-assembling mechanisms of the steps to construct nanoscale buildings on a surface. The dynamical mechanisms to cause step bunching are well known as follows; the step faceting[1], the electro-migration process[2]-[4], the Schwoebel effect[5, 6], the impurity effects[7, 8], and the process analogous to the traffic jam[9]. While, several thermodynamic mechanisms to cause step bunching near equilibrium has been found such as the strain-induced step bunching or strain-induced facet formation[10]-[16], the competition between the two surfaces with the different surface structures[17]-[20], and the thermal step bunching induced by adsorbates[21]-[30].

Recently, the first-order shape transition on the profile of the equilibrium crystal shape (ECS) $z = z(x, y)$ (Fig. 1) has been understood to be connected to the “thermal step bunching” on the vicinal surface[27]-[32]. The shape with the lowest surface free energy of a crystal particulate is called as ECS, which is determined by the anisotropic surface free energy[33]-[44]. The vicinal surfaces around the facet on the ECS are known to show the Gruber-Mullins-Pokrovski-Talapov (GMPT) universal behavior[45]-[70], having the universal form of the surface free energy per projected area $f(\mathbf{p})$ such as

$$f(p_x, p_y) = f(0, 0) + \gamma|\mathbf{p}|/d + B|\mathbf{p}|^3/d^3 + \mathcal{O}(|\mathbf{p}|^4), \quad (1)$$

where $\mathbf{p} = (p_x, p_y) = (\partial z(x, y)/\partial x, \partial z(x, y)/\partial y)$ represents the surface gradient, $|\mathbf{p}|$ represents $\sqrt{p_x^2 + p_y^2}$, $f(0, 0)$ represents the surface free energy of the surface with $|\mathbf{p}| = 0$, γ represents the step tension, B represents the step interaction coefficient, and d ($d = 1$) represents the height of a single step. We call $f(p_x, p_y)$ the vicinal surface free energy, hereafter.

As for the first-order transition on the profile of ECS, it was studied theoretically by several authors[71, 72, 73]. Rottman and Wortis[71] calculated the interface tension of the 3D cubic Ising model with next nearest neighbor (nnn) interaction by mean

field approximation. Jayaprakash *et. al.*[72, 73] studied the vicinal surface of a terrace-step-kink (TSK) model with the long range inter-step attraction. They calculated the surface free energy by means of mean field calculation, and showed that the profile of the ECS has the first-order transition due to the long range inter-step attraction. While, Akutsu *et al.*[21, 27, 28] showed that the small amount of adsorbates cause the first-order transition on the profile of the ECS on the restricted solid-on-solid (RSOS) model[74] couple with Ising system (RSOS-I model)[21, 27, 28].

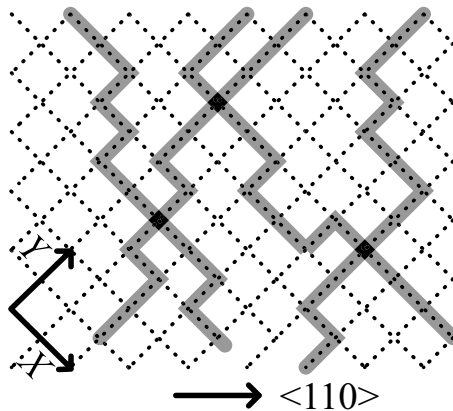


Figure 2. An example of the top view of the vicinal surface tilted relative to (001) surface along $\langle 110 \rangle$ direction. The gray lines represent surface steps. The filled squares represent the points where the adjacent steps collide.

In our previous paper[31, 32], we presented an RSOS model having inter-ledge attraction of the point contact type (p-RSOS model). The inter-ledge attraction expresses the transient bonding formed by the spatial overlap between orbitals at the collision point of the adjacent steps (Fig. 2). Experimentally, Ibach *et. al.*[16] suggested a short range inter-step attraction on the observation of the Cu surface. The inter-ledge attraction shown in Fig. 2 is the shortest one with respect to the range of interaction. Though the range of the interaction is short, the self-assembling of steps at low temperature near equilibrium is demonstrated by means of the Monte Carlo simulation on the vicinal surface of the p-RSOS model[31]. In addition, the first-order shape transition around (111) facet on the p-RSOS model[31] is obtained for the temperature T less than $T_{f,1}$ from the product wave-function renormalization group (PWFRG)[75]-[80] calculation, which is a variant of the density matrix renormalization group (DMRG)[81] calculation, of the Andreev surface free energy[39, 40] $\tilde{f}(\boldsymbol{\eta})$. The Andreev surface free energy is connected to the vicinal surface free energy $f(\mathbf{p})$ by the Legendre transformation such as $\tilde{f}(\boldsymbol{\eta}) = f(\mathbf{p}) - \mathbf{p} \cdot \boldsymbol{\eta}$. For the temperature $T \leq T_{f,2}$ ($< T_{f,1}$), (001) facet on the ECS directly contacts (111) facet on the ECS.

In the analysis of the ECS on the p-RSOS model for $T_{f,2} < T \lesssim T_{f,1}$, non-universal shape exponents are suggested in the PWFRG calculation. The aim of this paper is to clarify whether the profile around the (001) facet on the ECS shows universal behavior or not.

The paper is organized as follows. In §2, we present the p-RSOS model and give a brief explanation on the calculation method to obtain the surface quantities. In §3, we show the Andreev surface free energy, the gradient of the surface of the ECS around (001) facet, and the (001) facet contour calculated by the transfer matrix method with the PWFRG algorithm. The first-order shape transition on the profile of the ECS and the shape exponents around (001) facet are studied in detail. In §4, we make a detailed analysis of the formation of the step-droplets as the bunched steps near equilibrium. In §5, we derive the effective vicinal surface free energy where the step-droplets with various heights are taken into consideration. The general expressions for the shape exponents are also derived. The quasi non-universal shape exponents and other quantities obtained by PWFRG calculations are reproduced thermodynamically using the effective vicinal surface free energy. In §6 and §7, we give summary and conclusions.

2. p-RSOS model and the method of calculations

2.1. Model Hamiltonian

Let us consider the surface height $h(n, m)$ at the site (n, m) on the square lattice to describe the surface undulation microscopically. In the restricted solid-on-solid (RSOS) model[74], the height difference between nearest-neighbor (nn) sites are restricted to the values of $\{1, 0, -1\}$. We take into consideration the microscopic inter-ledge interaction of the point contact type (Fig. 2), and call the model p-RSOS model. Then the Hamiltonian of the p-RSOS model is written as follows:

$$\begin{aligned} \mathcal{H}_{\text{p-RSOS}} = & \sum_{n,m} \epsilon [|h(n+1, m) - h(n, m)| + |h(n, m+1) - h(n, m)|] \\ & + \sum_{n,m} \epsilon_{\text{int}} [\delta(|h(n+1, m+1) - h(n, m)|, 2) \\ & + \delta(|h(n+1, m-1) - h(n, m)|, 2)], \end{aligned} \quad (2)$$

where ϵ is the microscopic ledge energy, ϵ_{int} is the microscopic inter-ledge interaction energy, and $\delta(a, b)$ is Kronecker delta. The summation with respect to (n, m) is taken all over the sites on the square lattice. The RSOS restriction is required implicitly. In the case of $\epsilon_{\text{int}} < 0$, the surface structures which appear at the collision points of adjacent steps (Fig. 2) are favorable, since these structures have lower energy. Then, this inter-ledge attraction ($\epsilon_{\text{int}} < 0$) functions as the short range inter-step attraction.

For the vicinal surface, we add the terms of Andreev field[40] $\boldsymbol{\eta} = (\eta_x, \eta_y)$, which make surface be tilted, to the Hamiltonian Eq. (2). Accordingly, the model Hamiltonian Eq. (2) for the vicinal surface becomes as follows:

$$\begin{aligned} \mathcal{H}_{\text{vicinal}} = & \mathcal{H}_{\text{p-RSOS}} - \eta_x \sum_{n,m} [h(n+1, m) - h(n, m)] \\ & - \eta_y \sum_{n,m} [h(n, m+1) - h(n, m)]. \end{aligned} \quad (3)$$

The partition function \mathcal{Z} of the p-RSOS model is given as follows:

$$\mathcal{Z} = \sum_{\{h(m,n)\}} e^{-\beta \mathcal{H}_{\text{vicinal}}} \quad (4)$$

where $\beta = 1/k_{\text{B}}T$. The Andreev surface free energy $\tilde{f}(\boldsymbol{\eta})$ is the thermodynamic potential calculated from the partition function \mathcal{Z} as

$$\beta \tilde{f}(\boldsymbol{\eta}) = - \lim_{\mathcal{N} \rightarrow \infty} \frac{1}{\mathcal{N}} \ln \mathcal{Z}, \quad (5)$$

where \mathcal{N} is the number of lattice points on the square lattice.

2.2. Vertex model and transfer matrix method

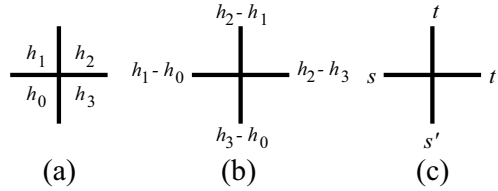


Figure 3. The mapping of the solid-on-solid model to the vertex model. (a) Surface configuration of the SOS model. (b) Mapping of the configuration to the vertex model. (c) Vertex model.

$$\begin{array}{cccccc}
 \begin{array}{c} 0 \\ | \\ 0 \end{array} \begin{array}{c} 0 \\ | \\ 0 \end{array} & \begin{array}{c} \pm 1 \\ | \\ 0 \end{array} \begin{array}{c} 0 \\ | \\ 0 \end{array} & \begin{array}{c} 0 \\ | \\ 0 \end{array} \begin{array}{c} \pm 1 \\ | \\ 0 \end{array} & \begin{array}{c} 0 \\ | \\ 0 \end{array} \begin{array}{c} 0 \\ | \\ \pm 1 \end{array} & \begin{array}{c} 0 \\ | \\ \pm 1 \end{array} \begin{array}{c} 0 \\ | \\ 0 \end{array} & \begin{array}{c} 0 \\ | \\ \mp 1 \end{array} \begin{array}{c} 0 \\ | \\ 0 \end{array} \\
 1 & \exp[-\beta \varepsilon] & \exp[-\beta \varepsilon] & \exp[-\beta \varepsilon] & \exp[-\beta \varepsilon] & \exp[-\beta(2\varepsilon + \varepsilon_{\text{int}})] \\
 \\
 \begin{array}{c} \pm 1 \\ | \\ 0 \end{array} \begin{array}{c} \pm 1 \\ | \\ 0 \end{array} & \begin{array}{c} 0 \\ | \\ 0 \end{array} \begin{array}{c} \pm 1 \\ | \\ \pm 1 \end{array} & \begin{array}{c} 0 \\ | \\ 1 \end{array} \begin{array}{c} 1 \\ | \\ 0 \end{array} & \begin{array}{c} 1 \\ | \\ 0 \end{array} \begin{array}{c} 0 \\ | \\ 1 \end{array} & & \begin{array}{c} \pm 1 \\ | \\ 0 \end{array} \begin{array}{c} 0 \\ | \\ \mp 1 \end{array} \\
 \exp[-\beta \varepsilon] & \exp[-\beta \varepsilon] & \exp[-2\beta \varepsilon] & \exp[-2\beta \varepsilon] & & \exp[-\beta(2\varepsilon + \varepsilon_{\text{int}})]
 \end{array}$$

Figure 4. Explicit surface configurations corresponding to the 19-vertices and their statistical weight.

In order to calculate Andreev free energy Eq. (5) statistically, we adopt the transfer-matrix method. We map the p-RSOS model (Eq. (2)) to the 19-vertex model[82] (Fig. 3) with the statistical weight shown in Fig. 4. For the vicinal surface, the statistical weight of each vertex is multiplied by $\exp[\beta\{(t + s')\eta_x + (s + t')\eta_y\}]$. We build the transfer matrix as shown in Fig. 5. From the largest eigen value of the transfer matrix, $\Lambda(N)$, where N is the number of the linked vertices, we have the Andreev surface free energy as

$$\beta \tilde{f}(\boldsymbol{\eta}) = - \lim_{M, N \rightarrow \infty} \frac{1}{NM} \ln \Lambda(N)^M, \quad (6)$$

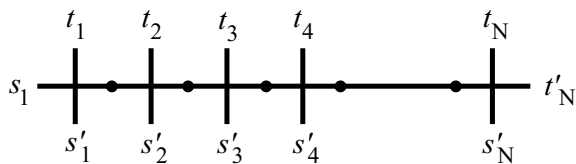


Figure 5. Transfer matrix made by linked vertices.

This figure is omitted for the file size limitation.

Figure 6. Perspective views of the reduced ECS around (001) facet calculated by the transfer matrix method with the PWFRG algorithm. $k_B T/\epsilon = 0.3$. (a) p-RSOS model ($\epsilon_{\text{int}}/\epsilon = -0.5$). (b) The original RSOS model ($\epsilon_{\text{int}} = 0$).

where M is the linear size of the system in the vertical-direction in Fig. 5.

For the efficient diagonalization of the transfer matrix, we employ PWFRG method[75]-[80]. In the PWFRG calculation, so called the number of the “retained bases” m are set from 7 to 37. The iteration number for the diagonalization is set to be $200 \sim 10^4$.

We calculated the surface gradient $\mathbf{p} = (p_x, p_y) = (\partial z/\partial x, \partial z/\partial y)$ as the thermal average of the height difference as follows:

$$\begin{aligned} p_x(\eta_x, \eta_y) &= \langle h(m+1, n) - h(m, n) \rangle d/a_x, \\ p_y(\eta_x, \eta_y) &= \langle h(m, n+1) - h(m, n) \rangle d/a_y, \end{aligned} \quad (7)$$

where $\langle \cdot \rangle$ represents the thermal average, and a_x and a_y represent the lattice constant for the x and y direction, respectively. We set $d = a_x = a_y = 1$. By sweeping the field $\boldsymbol{\eta}$, we obtain p_x v.s. η_x curve or p_y v.s. η_y curve[27, 28, 31, 32, 70, 82].

3. First-order transition on the profile of ECS

3.1. Andreev surface free energy

The Andreev surface free energy and Andreev field are connected to the coordinates of the ECS from the thermodynamics of the ECS[39, 40] as follows,

$$\tilde{f}(\eta_x, \eta_y) = \lambda z(x, y), \quad \eta_x = -\lambda x, \quad \eta_y = -\lambda y, \quad (8)$$

where λ is the Lagrange multiplier relating to the volume of the crystal particulate. The shape of $\tilde{f}(\eta_x, \eta_y)$ is similar to the ECS $z = z(x, y)$ (Fig. 1). Let us introduce the reduced ECS $Z = Z(X, Y)$, where $Z = \tilde{f}(\eta_x, \eta_y)/k_B T = \lambda z(x, y)/k_B T$, $X = \eta_x/k_B T = -\lambda x/k_B T$, and $Y = \eta_y/k_B T = -\lambda y/k_B T$. In Fig. 6, we show the perspective view of the calculated reduced ECS around the (001) surface at $k_B T/\epsilon = 0.3$. In the case of $\epsilon_{\text{int}} < 0$ (attractive inter-ledge interaction), large $\{111\}$ facets appears in addition to a (001) facet and $\{101\}$ facets. $\{111\}$ surface is stabilized energetically by ϵ_{int} , though the

microscopic inter-ledge attraction is local and transient. For comparison, we show the reduced ECS for the original RSOS model ($\epsilon_{\text{int}} = 0$) calculated by the PWFRG method in Fig. 6 (b).

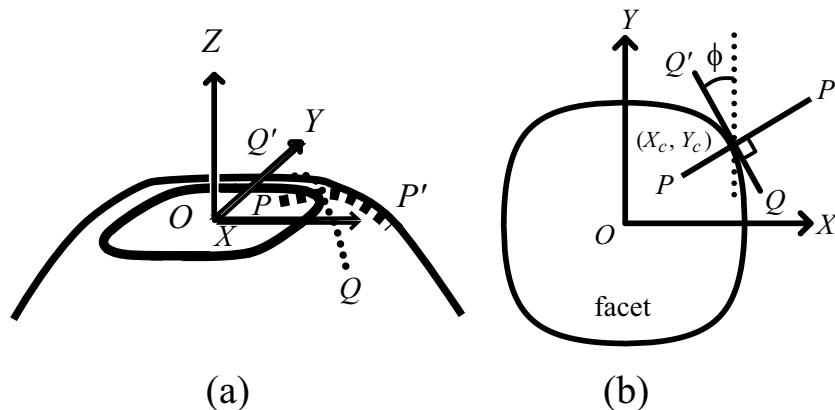


Figure 7. The normal line ($\overline{PP'}$) and the tangential line ($\overline{QQ'}$) around the (001) facet on the reduced ECS. (a) Perspective view. (b) Top view.

Let us consider the vicinal surface with the surface gradient $\mathbf{p} = (p_x, p_y)$ in the case of $p_y \neq 0$ near the facet contour of the ECS. \mathbf{p} is also expressed by $|\mathbf{p}|$ and ϕ such as $|\mathbf{p}| = \sqrt{p_x^2 + p_y^2}$, $p_x = |\mathbf{p}| \cos \phi$, and $p_y = |\mathbf{p}| \sin \phi$. The tangential line $\overline{QQ'}$ which contacts the facet contour at (X_c, Y_c) (Fig. 7) slants by the inclination angle ϕ relative to y -axis. Similarly, the normal line $\overline{PP'}$ which runs through (X_c, Y_c) also slants by the angle ϕ relative to x -axis. We parameterize the normal line by r and the tangential line by t such as

$$\begin{aligned} X &= X_c + r \cos \phi_0, & Y &= Y_c + r \sin \phi_0 & (\text{for } \overline{PP'}) \\ X &= X_c - t \sin \phi_0, & Y &= Y_c + t \cos \phi_0 & (\text{for } \overline{QQ'}), \end{aligned} \quad (9)$$

where ϕ_0 is the inclination angle ϕ at (X_c, Y_c) . Using (r, t) , we convert the components of the surface gradient from (p_x, p_y) to (p_r, p_t) like

$$p_r = p_x \cos \phi_0 + p_y \sin \phi_0, \quad p_t = -p_x \sin \phi_0 + p_y \cos \phi_0. \quad (10)$$

$|\mathbf{p}|$ and ϕ are also connected to (p_r, p_t) as $p_r = |\mathbf{p}| \cos(\phi - \phi_0)$ and $p_t = |\mathbf{p}| \sin(\phi - \phi_0)$. In the case of $\phi_0 = \pi/4$ ($a_x = a_y = 1$), we have

$$p_r = \sqrt{2}p_x, \quad p_t = (p_y - p_x)/\sqrt{2}. \quad (11)$$

We show the temperature dependence of the profile of the reduces ECS along the line $\overline{PP'}$ in Fig. 8. As seen from the figure, the curve between (001) facet and (111) facet shows the first-order shape transition at the edge of (111) facet (X_q, X_q) [31, 32]. Let us define the temperature $T_{f,1}$ as the highest temperature that the ECS causes the first-order transition on the profile of the ECS of the p-RSOS model. We obtain $k_B T_{f,1}/\epsilon = 0.3610 \pm 0.0005$ for $\epsilon_{\text{int}}/\epsilon = -0.5$ and $\phi = \pi/4$. In the temperature $T \leq T_{f,1}$, the first-order transition occurs at $X_q(T) = Y_q(T)$ on the profile of the ECS (Fig. 8

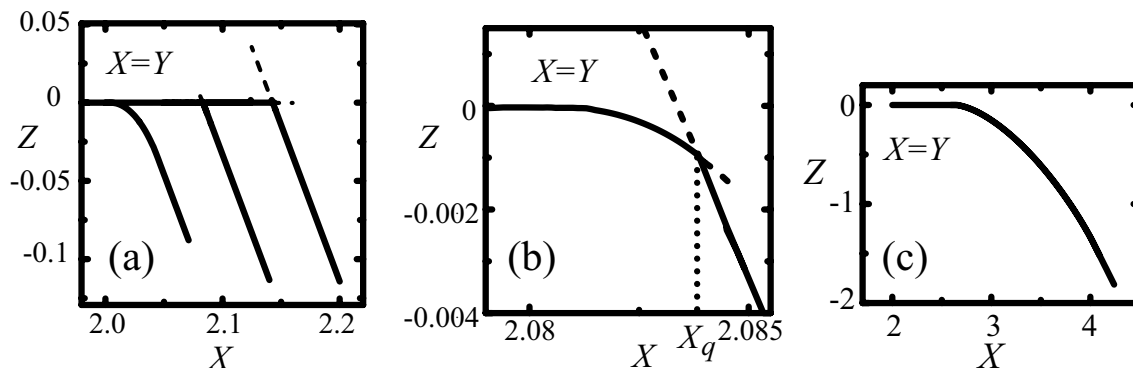


Figure 8. The profile of the reduced ECS along the line $\overline{PP'}$. $\phi = \pi/4$. $\epsilon_{\text{int}}/\epsilon = -0.5$. Broken lines show metastable lines. (a) From the right to left, $k_{\text{B}}T/\epsilon = 0.35, 0.36$, and 0.37 . (b) $k_{\text{B}}T/\epsilon = 0.36$. The edge of (111) facet is denoted by X_q . (c) The original RSOS model ($\epsilon_{\text{int}} = 0$). $k_{\text{B}}T/\epsilon = 0.3$.

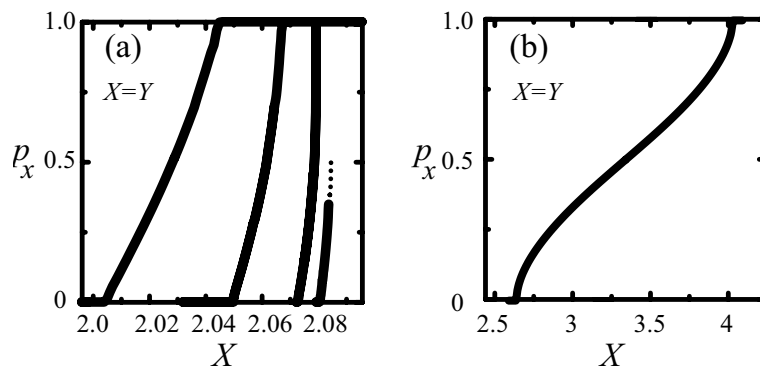


Figure 9. p_x v.s. X along the normal line $\overline{PP'}$ at $\phi = \pi/4$. (a) $\epsilon_{\text{int}}/\epsilon = -0.5$. From the right to left, $k_{\text{B}}T/\epsilon = 0.36, 0.361, 0.364$, and 0.37 . The broken line shows the p_x in the metastable state. (b) The original RSOS model. $\epsilon_{\text{int}} = 0$. $k_{\text{B}}T/\epsilon = 0.3$.

(b)). The surface slope jumps from $p_0 = 1$ to the p_1 at $X_q(T)$ with $0 \leq p_1 < 1$. We calculate $p_x(r)$ (Fig. 9) as a function of $X(r)$ by the PWFRG method along the line $\overline{PP'}$. In the case of $k_{\text{B}}T/\epsilon = 0.36$, $p_x(r)$ jumps from $p_1 = 0.349 \pm 0.002$ to $p_0 = 1$ at $X_q = Y_q = 2.084$ ($> X_c = Y_c = 2.0808 \pm 0.0002$). The values of p_x in the metastable state for $0.349 < p_x < 0.501$ are shown by the broken line in the figure.

Let us define the temperature $T_{f,2}$ as the temperature such that the curved area on the ECS in between (001) facet and (111) facet vanishes. We obtain $k_{\text{B}}T_{f,2}/\epsilon = 0.3585 \pm 0.0007$ for $\epsilon_{\text{int}}/\epsilon = -0.5$ and $\phi = \pi/4$. In the temperature $T \leq T_{f,2}$, (111) facet directly contacts (001) facet.

3.2. Equilibrium facet shape

In Fig. 10, we show the equilibrium facet shape (EFS) of the (001) facet. The values calculated by the PWFRG method[70] (X_c, Y_c) are shown by filled circles. Using the

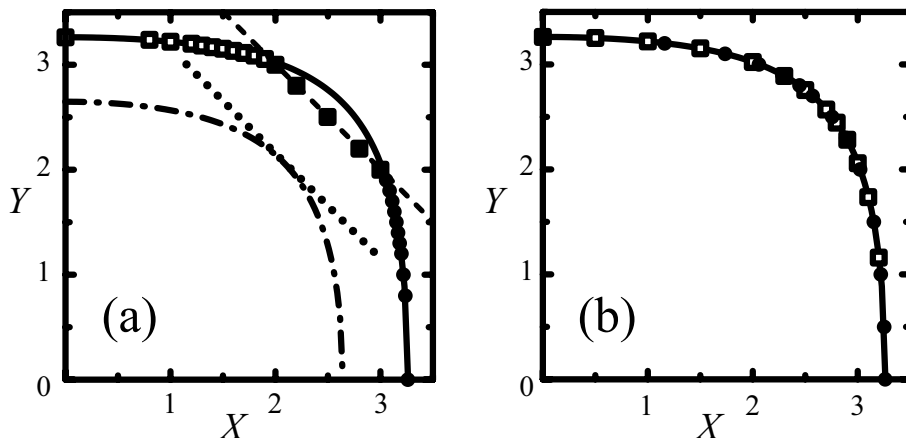


Figure 10. The equilibrium facet shape (EFS) for $X > 0$ and $Y > 0$. Full circle: (X_c, Y_c) calculated by the PWFRG method at $k_B T/\epsilon = 0.3$. Open square: (Y_c, X_c) . Full line: EFS for the 2D square nn Ising model (Eq. (14)) at $k_B T/\epsilon = 0.3$. Dash dotted line: EFS for the Ising model at $k_B T/\epsilon = 0.361$ (Eq. (14)). Dashed line: $Y = -X + 5.0$. Dotted line: $Y = -X + 4.1551$ (Eq. (15)). (a) $\epsilon_{\text{int}}/\epsilon = -0.5$. (b) $\epsilon_{\text{int}} = 0$.

symmetry, we plot (Y_c, X_c) by open squares. The full lines and the chain in Fig. 10 are the exactly obtained 2D ECS for the interface of the 2D square nn Ising model[83, 84, 51] at $k_B T/\epsilon = 0.3$ and $k_B T/\epsilon = 0.361$, respectively. The exact expression of the 2D ECS for the nn square Ising model is rewritten for the definition of the angle ϕ in Fig. 7 (b) as follows[85]-[90]:

$$D(X_c, Y_c) = 0, \quad \frac{\partial D(X, Y)}{\partial Y} \Big|_{(X, Y) = (X_c, Y_c)} = \tan \phi \frac{\partial D(X, Y)}{\partial X} \Big|_{(X, Y) = (X_c, Y_c)}, \quad (12)$$

where $D(X, Y)$ is

$$D(X, Y) = \cosh(X) + \cosh(Y) - \frac{\cosh^2(\epsilon/(k_B T))}{\sinh(\epsilon/(k_B T))}. \quad (13)$$

Hence, the equation of the ECS on the 2D square nn Ising model becomes as follows:

$$\cosh(X_c) + \cosh(Y_c) = \frac{\cosh^2(\epsilon/(k_B T))}{\sinh(\epsilon/(k_B T))}. \quad (14)$$

On the other hand, the dashed line and the dotted line in Fig. 10 (a) are the line of intersection between (001) surface and (111) surface on the ECS at $k_B T/\epsilon = 0.3$ and at $k_B T/\epsilon = 0.361$, respectively. They are calculated approximately from the following equation:

$$Y = -X + (2\epsilon + \epsilon_{\text{int}})/k_B T. \quad (15)$$

The facet shape obtained by the PWFRG calculations at $k_B T/\epsilon = 0.3$ agrees well with the 2D ECS for the 2D nn Ising model except for the part truncated by the line of intersection between (001) surface and (111) surface. As seen from the figure, $\gamma(\phi)$ on

the original RSOS model is well approximated by the interfacial tension on the 2D Ising model[83, 84, 51] (Fig. 10 (b)).

Let us calculate an approximate value of $T_{f,2}$. Since the vicinal surface energy of (111) surface amounts to $2\epsilon + \epsilon_{\text{int}}$ ($a_x = a_y = 1$), the truncation of the EFS is caused by the decrease of the surface energy of (111) surface due to ϵ_{int} . Therefore, in the case of $\epsilon_{\text{int}} < 0$, the EFS has the shape of the rounded square truncated by the line of intersection between (001) surface and (111) surface for $T < T_{f,2}$. Assuming $\phi^* = \pi/4$ and $X_c^* = Y_c^*$ where the line of intersection contacts the facet contour at $T = T_{f,2}^{(a)}$, we have $X_c^* = Y_c^* = (2\epsilon + \epsilon_{\text{int}})/(2k_B T_{f,2}^{(a)})$. Then substituting these quantities into Eq. (14), we have

$$\frac{\cosh^2(\epsilon/k_B T_{f,2}^{(a)})}{\sinh(\epsilon/k_B T_{f,2}^{(a)})} = 2 \cosh\left(\frac{2\epsilon + \epsilon_{\text{int}}}{2k_B T_{f,2}^{(a)}}\right). \quad (16)$$

By solving Eq. (16), we obtain $\epsilon/k_B T_{f,2}^{(a)} \approx 2.78778$ or $k_B T_{f,2}^{(a)}/\epsilon \approx 0.358709$, which is consistent with the PWFRG calculated value of $k_B T_{f,2}/\epsilon$ (§3.1).

3.3. Shape exponent

Let us define the “normal shape exponent” θ_n as the shape exponent[70] along the $\overline{PP'}$ in Fig. 7 (b) on the profile of the ECS such that $|Z(X(r), Y(r)) - Z(X_c, Y_c)| = \mathcal{A}_n(\phi)r^{\theta_n}$ ($0 \leq r$), where we call the coefficient $\mathcal{A}_n(\phi)$ as the “normal amplitude”. Similarly, let us define the “tangential shape exponent” θ_t and the “tangential amplitude” $\mathcal{A}_t(\phi)$ along the $\overline{QQ'}$ such that $|Z(X(t), Y(t)) - Z(X_c, Y_c)| = \mathcal{A}_t(\phi)|t|^{\theta_t}$.

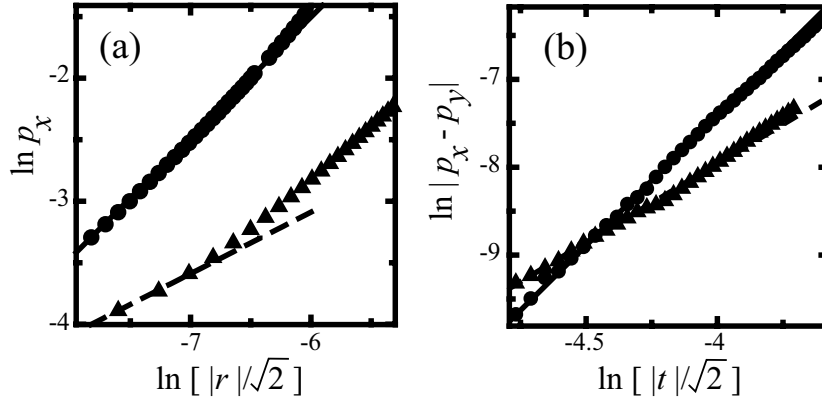


Figure 11. PWFRG calculated surface gradient. $\epsilon_{\text{int}}/\epsilon = -0.5$. $\phi = \pi/4$ Filled circle: $k_B T/\epsilon = 0.36$. Filled triangle: $k_B T/\epsilon = 0.37$. $X_c = Y_c = 2.0808$ for $k_B T/\epsilon = 0.36$, and $X_c = Y_c = 2.0051$ for $k_B T/\epsilon = 0.37$, (a) $\ln(p_x)$ *v.s.* $\ln[r/\sqrt{2}]$. Solid line: $\ln(p_x) = 0.98 \ln[r/\sqrt{2}] + 4.4$. Broken line: $\ln(p_x) = 0.500 \ln[r/\sqrt{2}] - 0.088$. (b) $\ln |p_x - p_y|$ *v.s.* $\ln[|t|/\sqrt{2}]$. Solid line: $\ln |p_x - p_y| = 2.96 \ln[|t|/\sqrt{2}] + 4.4$ Broken line: $\ln |p_x - p_y| = 1.8 \ln[|t|/\sqrt{2}] - 0.79$.

We show the logarithm of the calculated surface slope along the normal line in Fig. 11 (a), and the one along tangential line in Fig. 11 (b). The data of $k_B T/\epsilon = 0.36$ in

$-7.8 < \ln[r/\sqrt{2}] < -6.5$ for Fig. 11 (a) and in $-4.75 < \ln[|t|/\sqrt{2}] < -4$ for Fig. 11 (b) are fitted to the linear function $A_0 + A_1 \ln[r/\sqrt{2}]$ and $A'_0 + A'_1 \ln[|t|/\sqrt{2}]$ by the least square method, respectively. We obtain $A_1 = 0.98 \pm 0.03$, and $A_0 = 4.3 \pm 0.2$ for the normal direction and $A'_1 = 2.96 \pm 0.08$, and $A'_0 = 4.4 \pm 0.2$ for the tangential direction. From these values, we have $\theta_n = 1.98 \pm 0.03$, $\theta_t = 3.96 \pm 0.08$, $\mathcal{A}_n(\pi/4) = 40.6 \pm 0.2$, and $\mathcal{A}_t(\pi/4) = 7.2 \pm 1.0$. Both of the exponents disagree with the universal ones, where the universal values of the exponents are $\theta_n = 3/2$ and $\theta_t = 3$ [70].

At $k_B T/\epsilon = 0.37$, where $T_{f,1} < T$, the normal shape exponent with respect to the surface slope crosses over from a larger value to a smaller value. We draw a line which runs through the point $(-7.60, -3.89)$ in Fig. 11 (a) such as $\ln p_x = 0.5 \ln[r/\sqrt{2}] - 0.088$, and we show it by a broken line. The broken line agrees with the three calculated points from the smallest. Therefore, in the limit of $p_x \rightarrow 0$, we have $\theta_n = 1.5$ and $\mathcal{A}_n(\pi/4) = 0.73 \pm 0.04$. As for the profile along tangential line $\overline{QQ'}$, we have fitted the data in $-5 < \ln[|t|/\sqrt{2}] < -4.3$ to $A'_0 + A'_1 \ln[|t|/\sqrt{2}]$. We obtain $A'_1 = 1.8 \pm 0.3$ and $A'_0 = -0.79 \pm 0.08$, which leads to $\theta_t = 2.8 \pm 0.3$ and $\mathcal{A}_t(\pi/4) = 0.062 \pm 0.018$. From the values of θ_n and θ_t at $k_B T/\epsilon = 0.37$, we conclude that the profile near the (001) facet contour for $T > T_{f,1}$ and $\phi = \pi/4$ behaves like the GMPT universal one in the limit of $p_r \rightarrow 0$.

3.4. Step tension and step stiffness of a single step

Let us denote the step tension of the step with the mean running direction being parallel to the line $\overline{QQ'}$ by $\gamma(\phi)$ (Fig. 7). Similarly, let us denote the step interaction coefficient (Eq. 1) and the step stiffness by $B(\phi)$ and $\tilde{\gamma}(\phi) = \gamma(\phi) + \partial^2 \gamma(\phi)/\partial \phi^2$, respectively. From the thermodynamics of the ECS[40], the coordinates (X, Y) on the reduced ECS are obtained from $f(\mathbf{p})$ as follows[51];

$$X = \frac{1}{k_B T} \frac{\partial f(\mathbf{p})}{\partial p_x}, \quad Y = \frac{1}{k_B T} \frac{\partial f(\mathbf{p})}{\partial p_y}. \quad (17)$$

If we adopt the GMPT universal form for the surface free energy (Eq. (1)), $\gamma(\phi)$ is written by (X_c, Y_c) as

$$\gamma(\phi)/k_B T = X_c \cos \phi + Y_c \sin \phi, \quad (18)$$

since X_c and Y_c are connected to $f(\mathbf{p})$ from Eq. (17) in the limit of $|\mathbf{p}| \rightarrow 0$ like

$$\begin{aligned} X_c &= \frac{\gamma(\phi)}{k_B T} \cos \phi - \frac{1}{k_B T} \frac{\partial \gamma(\phi)}{\partial \phi} \sin \phi, \\ Y_c &= \frac{\gamma(\phi)}{k_B T} \sin \phi + \frac{1}{k_B T} \frac{\partial \gamma(\phi)}{\partial \phi} \cos \phi. \end{aligned} \quad (19)$$

The step tension and the step stiffness are well described by the interface tension and the interface stiffness of the 2D nn Ising model except for the orientation with respect to the truncated part in the facet contour. As shown in §3.2, the EFS calculated by the PWFRG method is well described by the 2D ECS of the 2D nn Ising model except for the truncated part of the EFS. The exact expressions of the interface tension

and the interface stiffness of the 2D nn Ising model are derived by use of $D(X, Y)$ (Eq. (12)) from Eq. (18) and

$$\begin{aligned} \tilde{\gamma}(\phi)_{\text{Ising}}/k_{\text{B}}T &= \left[\frac{\partial D(X, Y)}{\partial X} \cos \phi + \frac{\partial D(X, Y)}{\partial Y} \sin \phi \right] \\ &\times \left[\frac{\partial^2 D(X, Y)}{\partial X^2} \sin^2 \phi + \frac{\partial^2 D(X, Y)}{\partial Y^2} \cos^2 \phi \right. \\ &\left. - 2 \frac{\partial^2 D(X, Y)}{\partial Y \partial X} \sin \phi \cos \phi \right]^{-1} \Big|_{(X, Y)=(X_c, Y_c)}. \end{aligned} \quad (20)$$

Then, in the case of $\phi = \pi/4$, interface tension and interface stiffness for the 2D Ising model are exactly given as follows[83, 84, 51]:

$$\begin{aligned} \gamma\left(\frac{\pi}{4}\right)_{\text{Ising}}/k_{\text{B}}T &= \sqrt{2} \cosh^{-1} \left[\frac{\cosh^2(\beta\epsilon)}{2 \sinh(\beta\epsilon)} \right], \\ \tilde{\gamma}\left(\frac{\pi}{4}\right)_{\text{Ising}}/k_{\text{B}}T &= \sqrt{2} \tanh \left[\gamma\left(\frac{\pi}{4}\right)_{\text{Ising}}/(\sqrt{2}/k_{\text{B}}T) \right]. \end{aligned} \quad (21)$$

At $k_{\text{B}}T/\epsilon = 0.36$, we have $\gamma(\pi/4)_{\text{Ising}}/(\sqrt{2}k_{\text{B}}T) \approx 2.08075$, and $\tilde{\gamma}(\pi/4)_{\text{Ising}}/k_{\text{B}}T \approx 1.371$, and at $k_{\text{B}}T/\epsilon = 0.37$, we have $\gamma(\pi/4)_{\text{Ising}}/(\sqrt{2}k_{\text{B}}T) \approx 2.0051$, and $\tilde{\gamma}(\pi/4)_{\text{Ising}}/k_{\text{B}}T \approx 1.364$.

If we adopt the GMPT universal form for the surface free energy (Eq. 1), the gradient of the surface on the ECS is written by use of the step stiffness and the step interacting coefficient[52, 70] as follows;

$$p_r = \frac{1}{\sqrt{3\beta B(\phi)}} r^{1/2} \quad (\text{for } 0 \leq r), \quad p_t = \frac{1}{\sqrt{6\beta B(\phi)(\beta\tilde{\gamma}(\phi))^3}} t^2, \quad (22)$$

where $\beta = 1/k_{\text{B}}T$. If the systems has only short-range inter-step interactions, the coefficient $B(\phi)$ and the step stiffness satisfy the following universal relationship[52]

$$\beta B(\phi) = \frac{\pi^2}{6\beta\tilde{\gamma}(\phi)}. \quad (23)$$

Substituting Eq. (23) into Eq. (22), we have[70]

$$p_r = \frac{\sqrt{2\beta\tilde{\gamma}(\phi)}}{\pi} r^{1/2}, \quad p_t = \frac{1}{\pi\beta\tilde{\gamma}(\phi)} t^2. \quad (24)$$

In the case of $\phi = \pi/4$, Eq. (24) with Eq. (10) becomes

$$\begin{aligned} p_x &= p_r/\sqrt{2} = \frac{2}{u(\pi/4)\pi\sqrt{\pi}} |X - X_c|_{Y=X}^{1/2}, \\ |p_x - p_y|^{1/2} &= (\sqrt{2}p_t)^{1/2} = u\left(\frac{\pi}{4}\right) |X - X_c|_{Y=X_c+Y_c-X}, \end{aligned} \quad (25)$$

where

$$u\left(\frac{\pi}{4}\right) = \left[\frac{2\sqrt{2}}{\pi\beta\tilde{\gamma}(\pi/4)} \right]^{1/2}. \quad (26)$$

In above equation, we have used that r and t equal $\sqrt{2}(X - X_c)$.

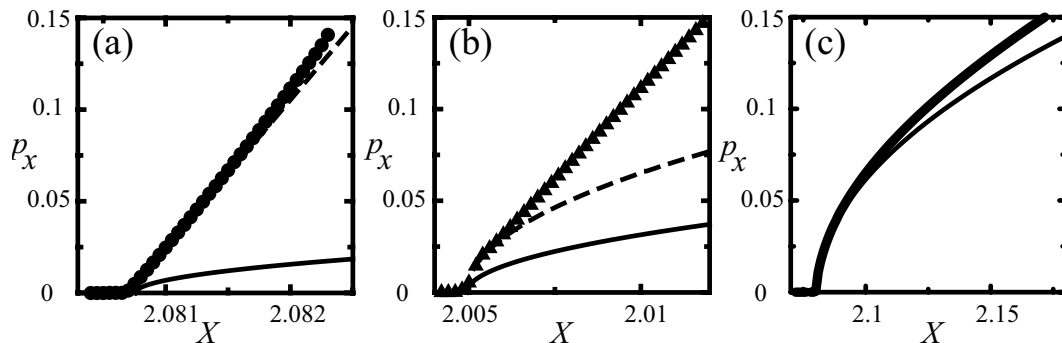


Figure 12. p_x v.s. X along the normal line $\overline{PP'}$. $\phi = \pi/4$. (a) $k_B T/\epsilon = 0.36$. $\epsilon_{\text{int}}/\epsilon = -0.5$. $X_c = Y_c = 2.0808$. Filled circles: PWFGR results. Thin solid line: $p_x = 0.4432\sqrt{X - X_c}$ for $X > X_c$ (Eq. (25)). Broken line: $p_x = 80.4X - 167.3$ (b) $k_B T/\epsilon = 0.37$. $\epsilon_{\text{int}}/\epsilon = -0.5$. $X_c = Y_c = 2.0051$. Filled triangles: PWFGR results. Thin solid line: $p_x = 0.4421\sqrt{X - X_c}$ for $X > X_c$. Broken line: $p_x = 0.9154\sqrt{X - X_c}$ for $X > X_c$. (c) The original RSOS model. $\epsilon_{\text{int}} = 0$. $k_B T/\epsilon = 0.36$. Thick solid line: PWFGR results. Thin solid line: $p_x = 0.4432\sqrt{X - X_c}$ for $X > X_c$.

In Fig. 12 (a), we show $p_x(r)$ for small p_r on the normal line $\overline{PP'}$. We draw line of Eq. (25) with Eq. (21) by thin solid line. As seen from the figure, the step tensions of a single step ($X_c = \gamma(\pi/4)/(\sqrt{2}k_B T)$) are well approximated by that of Ising model. For small p_x of the original RSOS model, the curve of p_x obtained by Eq. (25) with Eq. (21) expresses well as shown in Fig. 12 (c). On the other hand, p_x at $k_B T/\epsilon = 0.36$ largely differs from p_x calculated by Eq. (25) with Eq. (21) (Fig. 12 (a)). The best fitted curve obtained by the least-square method to the calculated data becomes $p_x = A_0 + A_1 X$ with $A_0 = 167.3 \pm 0.3$ and $A_1 = 80.4 \pm 0.2$ for small p_x . This curve is shown in Fig. 12 (a) by broken line.

In the case of $T_{f,1} < T$, at $k_B T/\epsilon = 0.37$ for example, the GMPT universal behavior is expected. In §3.3, we have shown that the shape exponents crossover to the universal values in the limit of $p_r \rightarrow 0$ (Fig. 11 (a)). Calculated p_x by the PWFGR method, however, differs from p_x calculated by Eq. (25) with Eq. (21) (Fig. 12 (b)). Using A_0 for $k_B T/\epsilon = 0.37$ obtained by the least square method in Fig. 11 (a), we draw the curve of $p_x = 0.9154\sqrt{X - X_c}$ by the broken line in Fig. 12 (b).

As for $T < T_{f,2}$, the orientation $\phi = \pi/4$ belongs to the truncated part in the facet contour. In that case, “a step” is realized not as the step with the unit height but as the bunched step with the step-height n . Accordingly, the step tension depends on n of “a single step”. In the large step-height limit, $\lim_{n \rightarrow \infty} \gamma_n(\pi/4)/n$ converges to $\sqrt{2}(\epsilon + \epsilon_{\text{int}}/2)$, which is smaller than $\gamma(\pi/4)_{\text{Ising}}$.

Let us consider the profile on the curve \overline{OP} (Fig. 13 (a)). We show, the calculated Andreev surface free energy and p_x - X curve in Fig. 13 (b) and (c), respectively. In the case of $\phi = 0$, Eq. (24) becomes

$$p_x = \frac{\sqrt{2\beta\tilde{\gamma}(0)}}{\pi}(X - X_c)^{1/2}|_{Y=0}, \quad p_y = \frac{1}{\pi\beta\tilde{\gamma}(0)}Y^2|_{X=X_c}, \quad (27)$$

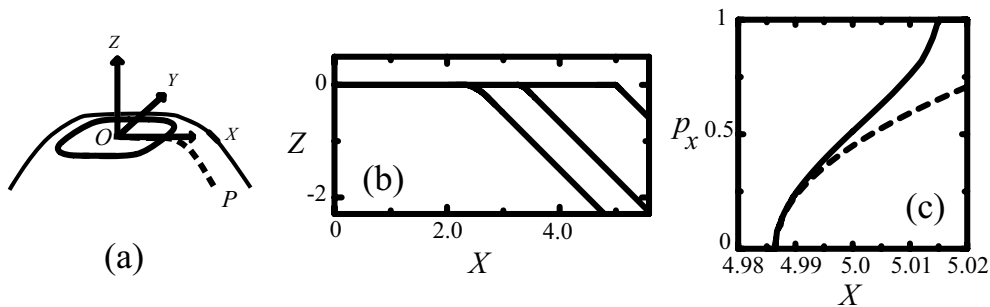


Figure 13. The profile of the reduced ECS along the curve \overline{OP} of the p-RSOS model. $\epsilon_{\text{int}}/\epsilon = -0.5$. (a) The schematic figure of the ECS and the curve \overline{OP} (broken line). (b) Andreev surface free energy over $k_B T$ (Z) *v.s.* X . From the right to left, $k_B T/\epsilon = 0.2, 0.3$, and 0.4 . (c) The surface slope p_x *v.s.* X . $k_B T/\epsilon = 0.2$. $X_c = 4.9865$, $Y_c = 0$. Broken line: p_x calculated by Eq. (27) with Eq. (28).

where $Y_c = 0$ and $X_c = 4.9865 \pm 0.0005$. The interface tension and the interface stiffness of Ising model are obtained exactly from Eq. (18) and Eq. (20) as follows:

$$\begin{aligned} \gamma(0)_{\text{Ising}}/k_B T &= \cosh^{-1} \left[\frac{\cosh^2(\epsilon/k_B T)}{\sinh(\epsilon/k_B T)} - 1 \right], \\ \tilde{\gamma}(0)_{\text{Ising}}/k_B T &= \sinh [\gamma(0)_{\text{Ising}}/k_B T]. \end{aligned} \quad (28)$$

The value of X_c agrees well with the $\gamma(0)_{\text{Ising}}/k_B T$. p_x calculated by Eq. (27) with Eq. (28) is shown by the broken line in Fig. 13 (c). As seen from the figure, the broken line well expresses the p_x - X curve calculated by the PWFRG method for small p_x . Therefore, the shape exponent for the normal line θ_n in this case becomes $\theta_n = 1.5$, which agrees with the GMPT universal behavior.

4. Step-droplets

4.1. Vicinal surface free energy

When the surface slope is chosen to be the external variable instead of the Andreev field $\boldsymbol{\eta}$, the thermodynamic function of the surface becomes the vicinal surface free energy $f(\mathbf{p})$, the surface free energy per projected area[39]. In the thermodynamic limit, $f(\mathbf{p})$ is calculated from $\tilde{f}(\boldsymbol{\eta})$ as follows;

$$f(\mathbf{p}) = \tilde{f}(\boldsymbol{\eta}) + \boldsymbol{\eta} \cdot \mathbf{p}. \quad (29)$$

Namely, using the notations on the reduced ECS, we have

$$f(\mathbf{p})/k_B T = Z + X p_x + Y p_y. \quad (30)$$

Obtained $f(\mathbf{p})$ of the p-RSOS model ($\epsilon_{\text{int}}/\epsilon = -0.5$) is shown in Fig. 14 (a), and $f(\mathbf{p})$ of the original RSOS model is shown in Fig. 14 (b). At $k_B T/\epsilon = 0.3$, only $f(0, 0)$ and $f(1, 1)$ are obtained by the PWFRG calculations, since the vicinal surface of the regular train of steps with $0 < p < 1$ is thermodynamically unstable. At $k_B T/\epsilon = 0.36$,

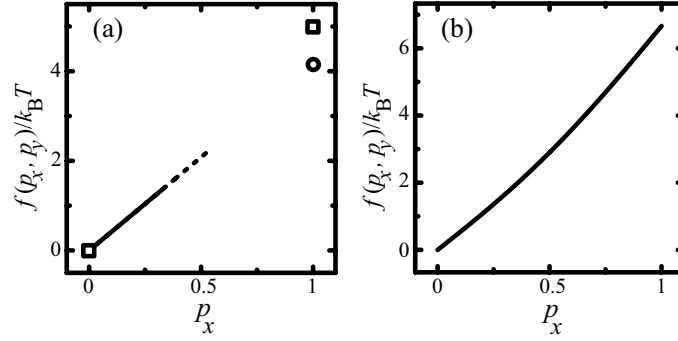


Figure 14. The surface free energy per projected area $f(\mathbf{p})$ (The vicinal surface free energy). (a) The p-RSOS model. $\epsilon_{\text{int}}/\epsilon = -0.5$. $p_x = p_y = p$. Full line: $f(p, p)$ at $k_B T/\epsilon = 0.36$. Dashed line: $f(p, p)$ at $k_B T/\epsilon = 0.36$ for the metastable state. Open circle: $f(1, 1)$ at $k_B T/\epsilon = 0.36$. Open square: $f(0, 0)$ and $f(1, 1)$ at $k_B T/\epsilon = 0.3$. (b) The original RSOS model ($\epsilon_{\text{int}} = 0$). Full line: $f(p, p)$ at $k_B T/\epsilon = 0.3$.

a curve of $f(\mathbf{p})$ is obtained for $0 \leq p_x \leq 0.349$, and the curve for the metastable state is obtained for $0.349 < p_x < 0.501$. For $k_B T/\epsilon = 0.3$ and 0.36 , $f(1, 1)$ is well approximated by $f(1, 1) = 2\epsilon + \epsilon_{\text{int}}$.

4.2. Thermal step bunching

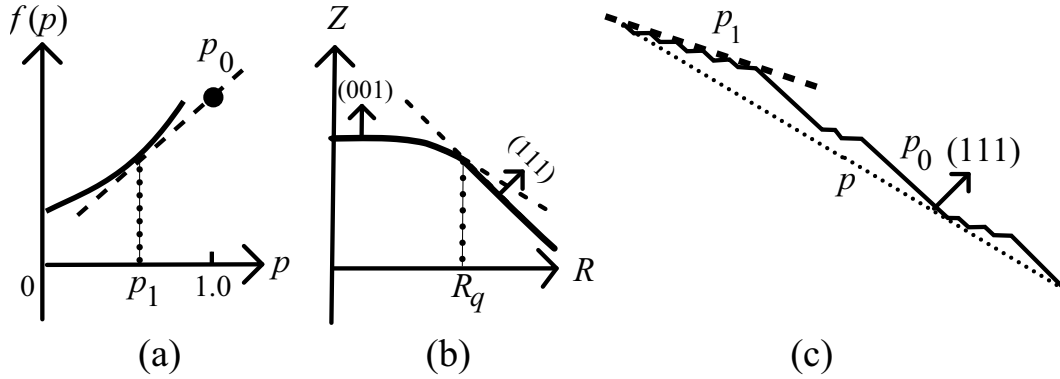


Figure 15. Thermal step bunching and the two surfaces coexistence. (a) The schematic figure of the vicinal surface free energy $f(p) \equiv f(p, p)$. Filled circle: $f(p_0) = f(1)$. Broken line: the tangential line connecting $(p_1, f(p_1))$ and $(p_0, f(p_0))$ with the line-slope = R_q (Eq.(32), (33)) [28]. (b) The schematic figure of the profile of the reduced ECS. $R = \sqrt{X^2 + Y^2}$. Broken line: the shape in the metastable state. The (111) facet edge, where the first-order transition occurs, is shown by R_q . The surface of the slope p_0 coexists with the surface of the slope p_1 at R_q . (c) An example of the step bunching as the two surfaces coexistence. Dotted line: mean surface slope ($= p$). Broken line: the local surface of the slope p_1 .

The first-order shape transition on the profile of the ECS (Fig. 15 (b)) leads to the coexistence of the two surfaces in the equilibrium (Fig. 15 (a)) [28, 29, 31], which we

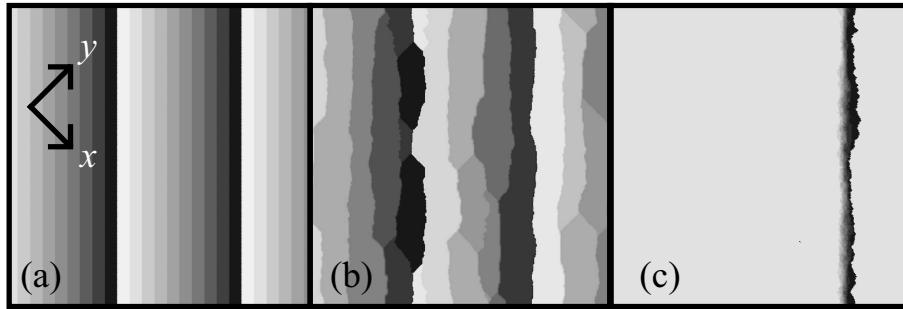


Figure 16. Snap shots of the simulated vicinal surfaces. Top view. $\epsilon_{\text{int}}/\epsilon = -0.5$. $240\sqrt{2} \times 240\sqrt{2}$. The height of the surface is described by the brightness with 10 gradations. The brighter, the higher. However, the brightness of the terrace on the left hand side of the brightest terrace, which is higher than the brightest by 1, becomes the darkest due to finite gradation. (a) Initial configuration. Number of steps: 24. (b) $k_{\text{B}}T/\epsilon = 0.1$. 5×10^6 MCS/cite. (c) $k_{\text{B}}T/\epsilon = 0.35$ (number of steps = 10). 4×10^8 MCS/cite.

call the thermal step bunching[27, 28]. Let us consider the free energy $\bar{f}(p)$ along the $\overline{PP'}$ in Fig. 7 for the mixture of surfaces with the slope p_0 and the ones with p_1 so that the mean surface slope becomes p . An example of the mixture of two kinds of surfaces is shown in Fig. 15 (c). The free energy of the simple mixed system is described as

$$\begin{aligned} \bar{f}(p) &= \bar{x}_1 f(p_1) + \bar{x}_0 f(p_0) \\ \bar{x}_1 + \bar{x}_0 &= 1 \end{aligned} \quad (31)$$

where \bar{x}_0 and \bar{x}_1 represents the ratio of the surface with the slope of p_0 and the one with p_1 , respectively. Since $\bar{x}_0 = (p - p_1)/(p_0 - p_1)$ and $\bar{x}_1 = (p_0 - p)/(p_0 - p_1)$, $\bar{f}(p)$ is rewritten as follows,

$$\bar{f}(p) = f(p_1) + \frac{[f(p_0) - f(p_1)]}{p_0 - p_1}(p - p_1). \quad (32)$$

Eq. (32) agrees with the expression of the co-tangent line which contacts $f(p)$ at the point $(p_0, f(p_0))$ and the point $(p_1, f(p_1))$ (see Fig. 15 (a)). Therefore, the free energy of the mixed surfaces has lower energy than the one of the homogeneous surface.

Further, from the thermodynamics of the ECS (Eq. (17)), we have

$$\begin{aligned} |\partial[f(p_x, p_y)/k_{\text{B}}T]/\partial p_r|_{p=p_0} &= |\partial[f(p_x, p_y)/k_{\text{B}}T]/\partial p_r|_{p=p_1} \\ &= R_q. \end{aligned} \quad (33)$$

Eq. (32) is rewritten as $\bar{f}(p) = f(p_1) + R_q(p - p_1)$. Consequently, we have

$$\bar{f}(p) + R_q p = f(p_1) + R_q p_1 = \tilde{f}(R_q). \quad (34)$$

4.3. Mean step-height

4.3.1. $T < T_{f,2}$ In the temperature $T < T_{f,2}$, the vicinal surface has the structure of the mixture of (111) surfaces and (001) surfaces. The structure is similar to the Herring's

hill and valley structure[28] or the Mullin's "step faceting"[1]. We demonstrate the "step faceting" by a Monte Carlo simulation. The examples of snap shots of the simulated vicinal surface are shown in Fig. 16. We consider the vicinal surface which inclines to (111) surface relative to (001) surface along $\langle 110 \rangle$ direction. The size of the system is $240\sqrt{2} \times 240\sqrt{2}$. The steps with the number of steps N_{step} lies on the surface at the same interval as the initial configuration (Fig. 16 (a)). We require periodic boundary condition for the vertical direction in Fig. 16. For the horizontal direction in Fig. 16, the surface height on the right side $h(i, j)$ ($h(240, 240)$, for example) are connected to the left side as $h(i', j') = h(i, j) + N_{\text{step}}$ ($h(0, 0) = h(240, 240) + N_{\text{step}}$, for example). As the time development, we adopt a simple Metropolis Algorithm with no driving force for the crystal growth. We choose a site (m, m') randomly. We also choose the direction of the change of the height $h(m, m')$, "addition" or "subtraction", with the probability 0.5. Then, the height is updated by the Metropolis algorithm under the RSOS restriction. That is, if the height differences among nn sites for the changed state equal $\{1, 0, -1\}$, the event occurs in the following probability P ;

$$P = \begin{cases} 1 & (\Delta E(m, m') \leq 0), \\ \exp[-\Delta E(m, m')/k_{\text{B}}T] & (\Delta E(m, m') > 0), \end{cases} \quad (35)$$

where $\Delta E(m, m') = E(h(m, m') \pm 1) - E(h(m, m'))$. The energy $E(h(m, m'))$ is calculated by Eq. (2).

In our previous paper[32], we demonstrate the zipping process in the early stage of the step bunching at the sufficiently low temperature (Fig. 16 (b)). The zipping process is the successive step sticking which starts from the colliding point of the adjacent steps like zipper on the clothes. Initially, the steps are set apart (Fig. 16 (a)) at the same interval. After starting the simulation, the steps travel and collide with adjacent steps due to thermal fluctuations. In order to see the zipping process in the simulated area, we choose temperature so that the "unzipping process" seldom occurs; and we choose the step-density (= the surface slope) so that the mean free length l_{free} with respect to the step-collision becomes to be less than the vertical size of the system ($240\sqrt{2}$).

As seen from the figure (Fig. 16 (b)), the multiple collision of steps occurs in the simulated area, and it causes several "bridges". The bridge is the single step connecting one bunched step to another bunched step. The zipping up movements come to an end when the bridge structure has the local minimum of the surface free energy. Hence, the vicinal surface stands still after a time τ_q . Namely, for $\tau_q \lesssim t$, the vicinal surface is quenched.

For slightly higher temperature where unzipping process occurs, with keeping the condition $T \leq T_{f,2}$, the vicinal surface reaches the configuration in the equilibrium (Fig. 16 (c)).

4.3.2. $T_{f,2} < T \leq T_{f,1}$ In order to get information on the bunched steps for $T_{f,2} < T \leq T_{f,1}$, we have measured the mean number of steps contained in a bunched step by the Monte Carlo method. The mean number of steps in a bunched step expresses

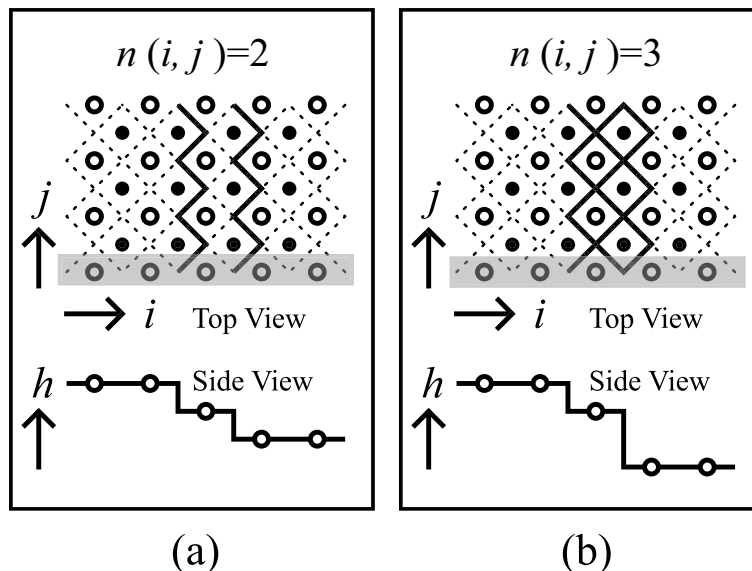


Figure 17. Schematic figure of the bunched step. Open circle: A-sublattice points. Closed circle: B-sublattice points. Upper figure: top view. Bottom figure: side view of the j -th row (shaded area) in the top view. Solid line (top view): surface steps. (a) $n(i, j) = 2$. (b) $n(i, j) = 3$.

the mean size of a step-droplet[28]. In order to calculate the size of a step-droplet in the Monte Carlo simulation, we divide the square lattice rotated by 45 degrees into two sub-lattices, which are represented by open circles and closed circles in the Fig. 17, respectively. Sweeping i from left to right under fixed j on the A-sublattice, we define a step-droplet at (i, j) as the configuration where the successive height difference starts from i at j -th row. The size of the step-droplet $n(i, j)$ is assigned as the step-height of the step-droplet, which also represents the number of steps contained in a step-droplet. The mean size of the step-droplets $\langle n \rangle$ is defined by

$$\langle n \rangle = \frac{1}{N_{\text{droplet}}} \sum_{j=1}^{N_j} \sum_{i=1}^{N_i} |n(i, j)|, \quad (36)$$

where $N_i = N_j = 240$ is the number of the unit lattice in i - and j - directions, respectively. N_{droplet} in the above is calculated by $N_{\text{droplet}} = \sum_{j=1}^{N_j} N_{\text{droplet}}(j)$, where $N_{\text{droplet}}(j)$ represents the number of step-droplets in the j -th row of the square lattice shown in Fig. 17.

In Fig. 18 (a), we show $\langle n \rangle$ calculated by the Monte Carlo method with the Metropolis algorithm (Eq. (35)). We have to take long time average up to 8×10^8 MCS/site at $k_B T / \epsilon = 0.36$ (open circles) due to large fluctuations of n . The Monte Carlo results shows that $\langle n \rangle$ increases linearly as p_r increases. The data are fitted to $\langle n \rangle = A_0 + A_1 p_r$ by the least square method, then obtained as $A_0 = 1.00 \pm 0.02$ and $A_1 = 2.26 \pm 0.08$. We draw figure of $\ln[\langle n \rangle - 1]$ *v.s.* $\ln p_r$ in Fig. 18 (b). Data for $p_r > 0.03$ are fitted to $\ln[\langle n \rangle - 1] = A_0 + A_1 \ln p_r$ by the least square method, which is shown by the upper solid line. We obtain $A_0 = 0.84 \pm 0.04$ and $A_1 = 1.00 \pm 0.02$.

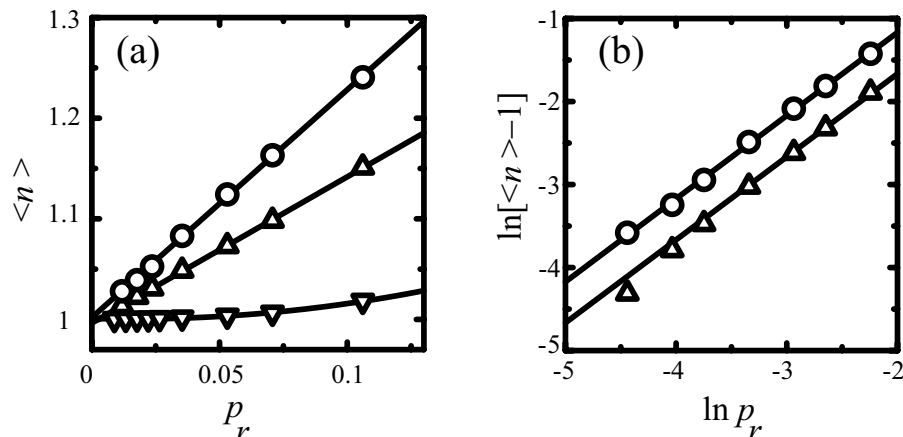


Figure 18. Slope dependence of the mean size of the step-droplets. Monte Carlo calculation. Lattice size: $240\sqrt{2} \times 240\sqrt{2}$. $\epsilon_{\text{int}}/\epsilon = -0.5$. Circle: $k_{\text{B}}T/\epsilon = 0.36$, 8×10^8 MCS/site. Triangle: $k_{\text{B}}T/\epsilon = 0.37$, 4×10^8 MCS/site. Reversed triangle: $k_{\text{B}}T/\epsilon = 0.36$, $\epsilon_{\text{int}} = 0$ (original RSOS model), 2×10^8 MCS/site.

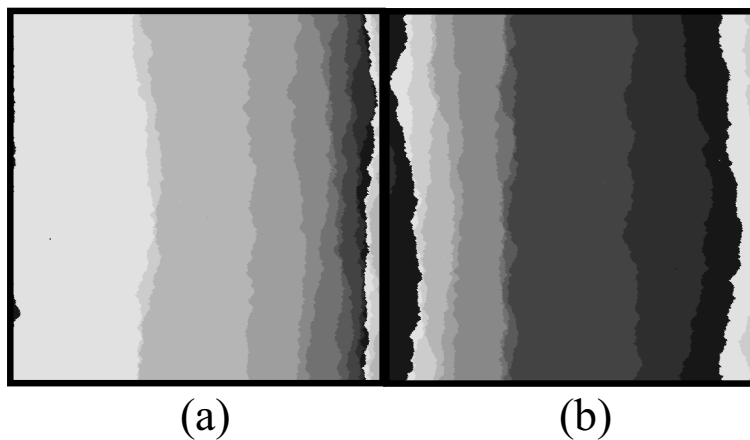


Figure 19. Snap shots of the simulated vicinal surfaces. Top view. $\epsilon_{\text{int}}/\epsilon = -0.5$. 4×10^8 MCS/site. $240\sqrt{2} \times 240\sqrt{2}$. Number of steps: 12. The height of the surface is described by the brightness with 10 gradations. The brighter, the higher. (a) $k_{\text{B}}T/\epsilon = 0.36$. (b) $k_{\text{B}}T/\epsilon = 0.37$.

As seen from the figure, the data for $p_r < 0.03$ agrees well with the line. We show an example of the step-droplets at $k_{\text{B}}T/\epsilon = 0.36$ in Fig. 19 (a).

4.3.3. $T_{f,1} < T$ In this temperature region, the GMPT universal behavior is expected. As seen from Fig. 18, however, simple universal behavior like the original RSOS model (reversed open triangles) is not obtained at $k_{\text{B}}T/\epsilon = 0.37$ (open triangles). In the case of the original RSOS model, obtained data are fitted to $\langle n \rangle = A_0 + A_1 p_r + A_2 p_r^2$ by the least square method. We have $A_0 = 1.001 \pm 0.008$, $A_1 = -0.07 \pm 0.09$, and $A_2 = 2.2 \pm 1.0$. These values suggest $A_0 = 1$ and $A_1 = 0$ for the GMPT universal system in the limit

of $p_r \rightarrow 0$. While for p-RSOS model, $\langle n \rangle$ seems to increase linearly as p_r increases at $k_B T/\epsilon = 0.37$. In Fig. 18 (a), the data at $k_B T/\epsilon = 0.37$ are fitted to $\langle n \rangle = A'_0 + A'_1 p_r$, and we have $A'_0 = 0.996 \pm 0.04$ and $A'_1 = 1.45 \pm 0.03$. From Fig. 18 (b), the data at $k_B T/\epsilon = 0.37$ for $p_r > 0.03$ are fitted to $\ln(\langle n \rangle - 1) = A''_0 + A''_1 \ln p_r$, and we have $A''_0 = 0.58 \pm 0.5$ and $A''_1 = 1.09 \pm 0.07$. The value of A''_1 which is slightly larger than 1 may suggest the cross over from the non-universal behavior to the universal one as p_r decreases. We show an example of the snap shots (Fig. 19 (b)) at $k_B T/\epsilon = 0.37$. In the figure, we can see the small size of bunched steps (step-droplets).

5. Quasi non-universal behavior

5.1. Derivation of the quasi non-universal vicinal surface free energy

Let us consider the case where a bunched step can be regarded as a single step. We denote the step-density of the bunched step with the step-height being n by ρ_n . We assume that the interaction among bunched steps is the short range. Then, the vicinal surface free energy $f_n(\rho_n)$ of the vicinal surface made up from the bunched step with the step-height n becomes the GMPT universal type as follows,

$$f_n(\rho_n) = f(0) + \gamma_n(\phi)\rho_n + B_n(\phi)\rho_n^3 + C_n(\phi)\rho_n^4 + \mathcal{O}(\rho_n^5), \quad (37)$$

where $\gamma_n(\phi)$ represents the step tension of the bunched step, $B_n(\phi)$ represents the step interaction coefficient among bunched steps, $C_n(\phi)$ is the coefficient with respect to ρ_n^4 .

Let us investigate n dependence of $f_n(\rho_n)$ in the limit of $\rho_n \rightarrow 0$. ρ_n is expressed as $\rho_n = N_{s,n}/L = |\mathbf{p}|/d_n$, where $N_{s,n}$ is the total number of bunched steps of the step-height n , L is the linear length of the projected area of the vicinal surface, and d_n is the height of the bunched step. L is assumed to be sufficiently large so that we may take thermodynamic limit. Substituting the expressions of ρ_n and $d_n = nd_1$ into Eq. (37), we have

$$f_n(\mathbf{p}) = f(0) + \frac{\gamma_n(\phi)}{d_1 n} |\mathbf{p}| + \frac{B_n(\phi)}{d_1^3 n^3} |\mathbf{p}|^3 + \frac{C_n(\phi)}{d_1^4 n^4} |\mathbf{p}|^4 + \mathcal{O}(p^5). \quad (38)$$

Since $\gamma_n(\phi)$ is considered to be $n\gamma_1(\phi)$ approximately, we expand $\gamma_n(\phi)/n$ with respect to n around $n = 1$ as follows;

$$\begin{aligned} \frac{\gamma_n(\phi)}{n} &= \gamma_1(\phi) + \gamma_1^{(1)}(\phi)(n-1) + \frac{1}{2}\gamma_1^{(2)}(\phi)(n-1)^2 + \dots \\ \gamma_1^{(m)}(\phi) &= \left. \frac{\partial^m (\gamma_n(\phi)/n)}{\partial n^m} \right|_{n=1} \end{aligned} \quad (39)$$

The universal relationship between $B_n(\phi)$ and $\tilde{\gamma}_n(\phi)$ like Eq. (23) is assumed to hold as follows;

$$\frac{B_n(\phi)}{k_B T} = \frac{\pi^2 k_B T}{6\tilde{\gamma}_n(\phi)} \quad (40)$$

where $\tilde{\gamma}_n(\phi)$ represents the step stiffness of the bunched step ($\tilde{\gamma}_n(\phi) = \gamma_n(\phi) + \partial^2 \gamma_n(\phi)/\partial \phi^2$). Accordingly, instead of expanding $B_n(\phi)$ with respect to n , we expand

$\tilde{\gamma}_n(\phi)$ like $\gamma_n(\phi)$ around $n = 1$, that is,

$$\begin{aligned} \frac{\tilde{\gamma}_n(\phi)}{n} &= \tilde{\gamma}_1(\phi) + \tilde{\gamma}_1^{(1)}(\phi)(n-1) + \frac{1}{2}\tilde{\gamma}_1^{(2)}(\phi)(n-1)^2 + \dots \\ \tilde{\gamma}_1^{(m)}(\phi) &= \left. \frac{\partial^m(\tilde{\gamma}_n(\phi)/n)}{\partial n^m} \right|_{n=1}. \end{aligned} \quad (41)$$

Substituting Eq. (39) and Eq. (41) into Eq. (38) together with the relationship Eq. (40), we have

$$\begin{aligned} f_n(\mathbf{p}) &= f(0) + \left[\gamma_1(\phi) - \gamma_1^{(1)}(\phi) + \frac{\gamma_1^{(2)}(\phi)}{2} \right. \\ &+ \left. (\gamma_1^{(1)}(\phi) - \gamma_1^{(2)}(\phi))n + \frac{\gamma_1^{(2)}(\phi)}{2}n^2 \right] \frac{|\mathbf{p}|}{d_1} \\ &+ \frac{B_1(\phi)}{n^4} \frac{|\mathbf{p}|^3}{d_1^3} \left[1 + (n-1) \frac{\tilde{\gamma}_1^{(1)}(\phi)}{\tilde{\gamma}_1(\phi)} + \frac{1}{2}(n-1)^2 \frac{\tilde{\gamma}_1^{(2)}(\phi)}{\tilde{\gamma}_1(\phi)} \right]^{-1} \\ &+ \frac{C_n(\phi)}{n^4} \frac{|\mathbf{p}|^4}{d_1^4} + \mathcal{O}(|\mathbf{p}|^5). \end{aligned} \quad (42)$$

Then, we approximate Eq. (42) by replacing n with $\langle n(\phi) \rangle$. As mentioned in §4.3, $\langle n(\phi) \rangle$ depends on \mathbf{p} . Hence, we expand $\langle n(\phi) \rangle$ with respect to $|\mathbf{p}|$ around $|\mathbf{p}| = 0$. Namely,

$$\begin{aligned} \langle n \rangle &= 1 + n_0^{(1)}(\phi)|\mathbf{p}| + \frac{1}{2}n_0^{(2)}(\phi)|\mathbf{p}|^2 + \frac{1}{6}n_0^{(3)}(\phi)|\mathbf{p}|^3 + \dots \\ n_0^{(m)}(\phi) &= \left. \frac{\partial^m \langle n(\phi) \rangle}{\partial |\mathbf{p}|^m} \right|_{|\mathbf{p}|=0+}. \end{aligned} \quad (43)$$

Substituting Eq. (43) into Eq. (42), and after some calculations, we have the final form of vicinal surface free energy as follows:

$$\begin{aligned} f_{\text{eff}}(\mathbf{p}) \equiv f_{\langle n \rangle}(\mathbf{p}) &= f(0) + \gamma_1(\phi) \frac{|\mathbf{p}|}{d_1} + A_{\text{eff}}(\phi)|\mathbf{p}|^2 \\ &+ B_{\text{eff}}(\phi)|\mathbf{p}|^3 + C_{\text{eff}}(\phi)|\mathbf{p}|^4 + \mathcal{O}(|\mathbf{p}|^5), \end{aligned} \quad (44)$$

where

$$A_{\text{eff}}(\phi) = n_0^{(1)}(\phi)\gamma_1^{(1)}(\phi)/d_1 \quad (45)$$

$$B_{\text{eff}}(\phi) = \frac{1}{2d_1} \left[n_0^{(2)}(\phi)\gamma_1^{(1)}(\phi) + n_0^{(1)}(\phi)\gamma_1^{(2)}(\phi) \right] + \frac{B_1(\phi)}{d_1^3} \quad (46)$$

$$\begin{aligned} C_{\text{eff}}(\phi) &= \frac{1}{6d_1} \left[n_0^{(3)}(\phi)\gamma_1^{(1)}(\phi) + 3n_0^{(1)}(\phi)n_0^{(2)}(\phi)\gamma_1^{(2)}(\phi) \right] \\ &- \frac{B_1(\phi)n_0^{(1)}(\phi)}{d_1^3} \left(6 + \frac{\tilde{\gamma}_1^{(1)}(\phi)}{\tilde{\gamma}_1(\phi)} \right) + \frac{C_n(\phi)}{d_1^4}. \end{aligned} \quad (47)$$

We regard $d_1 = 1$, hereafter. It is interesting that $f_{\text{eff}}(\mathbf{p})$ have the quadratic term with respect to $|\mathbf{p}|$ due to step-droplets. The step-droplets also cause $B_{\text{eff}}(\phi)$ to be different from $B_1(\phi)$.

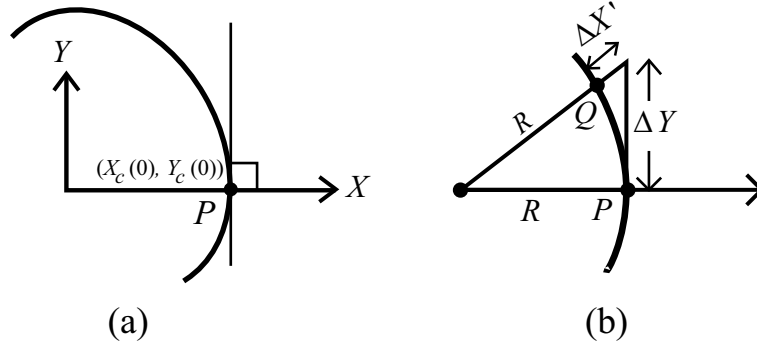


Figure 20. (a) Choice of X - and Y -axes at P on the facet contour. (b) Q lies near P on the facet contour. “normal distance” $\Delta X'$ relates to “tangential distance” ΔY as $\Delta X' = (\Delta Y)^2/2R$, where R is the radius of curvature at P .

5.2. Scaling relation between shape exponents

Let us derive the expressions of the shape exponents extended to the case of the $f(\mathbf{p})$ having the non-universal form such as

$$f(\mathbf{p}) = f(0) + \gamma(\phi)|\mathbf{p}| + B_\zeta(\phi)|\mathbf{p}|^\zeta + O(|\mathbf{p}|^{\zeta+1}), \quad (48)$$

where $\zeta > 1$. From Eq. (17), the reduced coordinates (X, Y) on the ECS are written

$$\begin{aligned} X &= X_c(\phi) + |\mathbf{p}|^{\zeta-1} \left[\frac{\zeta B_\zeta(\phi)}{k_B T} \cos \phi - \frac{B'_\zeta(\phi)}{k_B T} \sin \phi \right], \\ Y &= Y_c(\phi) + |\mathbf{p}|^{\zeta-1} \left[\frac{\zeta B_\zeta(\phi)}{k_B T} \sin \phi + \frac{B'_\zeta(\phi)}{k_B T} \cos \phi \right], \\ B'_\zeta(\phi) &= \partial B_\zeta(\phi)/\partial \phi, \end{aligned} \quad (49)$$

where $(X_c(\phi), Y_c(\phi))$ is obtained by Eq. (19). In the following, we consider the case where the first-order shape transition does not occur on the facet contour of (001) facet. Let us choose X - and Y - axes so that Y -axis is parallel to the tangential line of the facet contour at P (Fig. 20). With this choice of the coordinate system, we have $\phi = 0$ at P and $\gamma'(0) = 0$ (Eq. (19)). Along the tangential line ($X = X_c(0) = 0$), ϕ and $|\mathbf{p}|$ are not independent but are constrained to satisfy,

$$-\frac{1}{2}\tilde{\gamma}(0)\phi^2 + \zeta B_\zeta(0)|\mathbf{p}|^{\zeta-1} = 0, \quad (50)$$

which is derived by expanding (49) and (19) with respect to ϕ and $|\mathbf{p}|$ ($|\mathbf{p}| \ll 1$ and $|\phi| \ll 1$, near the point P). Combining (50) with (49) and (19), we obtain

$$\phi = \frac{k_B T \Delta Y}{\tilde{\gamma}(0)}, \quad |\mathbf{p}| = \left[\frac{(k_B T)^2 \Delta Y^2}{2\zeta \tilde{\gamma}(0) B_\zeta(0)} \right]^{\frac{1}{\zeta-1}} \quad (51)$$

along the tangential line \overline{PQ} in Fig. 20, where $\Delta Y = Y - Y_c$. Near P , $Z = \tilde{f}(X_c(0), \Delta Y + Y_c(0))/k_B T$ is expanded to give

$$\Delta Z = -\frac{[\gamma(0) + \frac{1}{2}\gamma''(0)\phi^2]}{k_B T} |\mathbf{p}| + \frac{B_\zeta(0)}{k_B T} |\mathbf{p}|^\zeta$$

$$-\Delta Y |\mathbf{p}| \phi - X_c(0) |\mathbf{p}| \left(1 - \frac{1}{2} \phi^2\right), \quad (52)$$

where $\Delta Z = Z(X, Y) - Z(X_c, Y_c)$. Putting (51) into (52), we have expressions for the tangential shape exponent θ_t and the tangential amplitude $\mathcal{A}_t(\phi)$ as follows:

$$\begin{aligned} \Delta Z &= -\mathcal{A}_t(0) |\Delta Y|^{\theta_t}, \\ \mathcal{A}_t(0) &= \frac{1}{\theta_t} \left[\frac{(k_B T)^{\zeta+1}}{2\zeta B_\zeta(0) \tilde{\gamma}(0)^\zeta} \right]^{\frac{1}{\zeta-1}}, \quad \theta_t = 2\zeta/(\zeta - 1). \end{aligned} \quad (53)$$

Similarly, along the normal line ($Y - Y_c(0) = 0$), we have expressions for the normal amplitude $\mathcal{A}_n(\phi)$ and the normal shape exponent θ_n as follows:

$$\begin{aligned} \Delta Z &= -\mathcal{A}_n(0) (\Delta X)^{\theta_n}, \quad (X_c(0) \leq X) \\ \mathcal{A}_n(0) &= \frac{1}{\theta_n} \left[\frac{k_B T}{\zeta B_\zeta(0)} \right]^{\frac{1}{\zeta-1}}, \quad \theta_n = \zeta/(\zeta - 1). \end{aligned} \quad (54)$$

From Eq. (53) and Eq. (54), we have a scaling relation like

$$\theta_t = 2\theta_n \quad (55)$$

when $\tilde{\gamma}(0) \neq 0$. From Eq. (54) and Eq. (53), we obtain following relation

$$\Delta X = \left[\frac{\mathcal{A}_t(0)}{\mathcal{A}_n(0)} \right]^{\frac{1}{\theta_n}} \Delta Y^2 = \frac{k_B T}{2\tilde{\gamma}(0)} \Delta Y^2. \quad (56)$$

This expression is also obtained geometrically from Fig. 20 (b) using the radius of curvature R such as $\Delta X' = \Delta Y^2/(2R) = k_B T \Delta Y^2/(2\tilde{\gamma}(0))$ [83] and $\Delta X' = \Delta X$ for small $\Delta X'$ and ΔY .

5.3. Gaussian curvature

Let us discuss Gaussian curvature around the facet on the reduced ECS. The first fundamental quantity[44, 91] $g_{\mu\nu}$ ($\mu, \nu = 1, 2$) of surface is given by $g_{\mu\nu} = \delta_{\mu\nu} + p_\mu \cdot p_\nu$, where $\delta_{\mu\nu}$ the Kronecker delta, $p_1 = p_x$, and $p_2 = p_y$. In the limit of $|\mathbf{p}| \rightarrow 0$, $g_{\mu\nu}$ becomes $\delta_{\mu\nu}$, and the curvature tensor is obtained from the second fundamental quantity $H_{\mu\nu}$ [44, 91], which is given by $H_{\mu\nu} = -(1/\sqrt{g}) \partial^2 Z(\mathbf{X})/\partial X^\mu \partial X^\nu$, where $g = \det(g_{\mu\nu})$, $X^1 = X$ and $X^2 = Y$. The Gaussian curvature K on the surface of the reduced ECS is given by $K = \det(H_{\mu\nu})/g$.

$H_{\mu\nu}$ is also written by use of the (surface) stiffness tensor $f^{ij} = \partial^2 f(\mathbf{p})/\partial p_i \partial p_j$ as $(H_{ij}) = (-k_B T/\sqrt{g})(f^{ij})^{-1}$ [44]. Adopting Eq. (48) as the form of $f(\mathbf{p})$, and thinking of Eq. (17) together with Eq. (49) and Eq. (19), we obtain the explicit expressions of f^{ij} as follows:

$$f^{11} = \frac{\tilde{\gamma}}{p} \sin^2 \phi + p^{\zeta-2} (t_1 - t_2 \sin^2 \phi - 2t_3 \sin \phi \cos \phi), \quad (57)$$

$$f^{22} = \frac{\tilde{\gamma}}{p} \cos^2 \phi + p^{\zeta-2} (t_4 + t_2 \sin^2 \phi + 2t_3 \sin \phi \cos \phi), \quad (58)$$

$$\begin{aligned}
 f^{12} &= -\frac{\tilde{\gamma}}{p} \sin \phi \cos \phi + p^{\zeta-2} [t_3(1 - 2 \sin^2 \phi) + t_2 \sin \phi \cos \phi] \\
 &= f^{21},
 \end{aligned} \tag{59}$$

$$\det(f^{ij}) = t_1 p^{\zeta-3} \tilde{\gamma}(\phi) + p^{2\zeta-4} (t_1 t_4 - t_3^2), \tag{60}$$

where $p = |\mathbf{p}|$, t_1 , t_2 , t_3 , and t_4 represent

$$\left. \begin{aligned}
 t_1 &= \zeta(\zeta - 1)B_\zeta(\phi) \\
 t_2 &= \zeta(\zeta - 2)B_\zeta(\phi) - B_\zeta''(\phi) \\
 t_3 &= (\zeta - 1)B_\zeta'(\phi) \\
 t_4 &= \zeta B_\zeta(\phi) + B_\zeta''(\phi). \\
 B_\zeta''(\phi) &= \partial^2 B_\zeta(\phi) / \partial \phi^2
 \end{aligned} \right\} \tag{61}$$

Here, we have neglected higher order terms with respect to p . Using this stiffness tensor, we obtain the Gaussian curvature of the reduced ECS near the facet edge by the expression $K = \det(H_{ij})/g = (k_B T)^2 / (g^2 \det(f^{ij}))$. Hence, we have

$$K = \frac{(k_B T)^2 p^{3-\zeta}}{\zeta(\zeta - 1)B_\zeta(\phi)\tilde{\gamma}(\phi)}. \tag{62}$$

In the universal case ($\zeta = 3$), for example, together with the universal relationship $6\tilde{\gamma}(\phi)B_3(\phi) = \pi^2(k_B T)^2[52]$, we have K as $K = 1/\pi^2$ ($p \rightarrow 0_+$). Since the Gaussian curvature on the facet equals 0, the Gaussian curvature jumps at the facet edge from zero to $1/\pi^2[52]$.

5.4. Quasi non-universal shape exponents

Based on the PWFRG results, we discuss the quasi non-universal behavior on the ECS near (001) facet. From the vicinal surface free energy Eq. (44) and the thermodynamic relations of (X, Y) (Eq. (17)), we have the equations on the ECS as follows:

$$\begin{aligned}
 X &= X_c^{(g)} + \frac{1}{k_B T} \left[2A_{\text{eff}}(\phi) \cos \phi - \frac{\partial A_{\text{eff}}(\phi)}{\partial \phi} \sin \phi \right] |\mathbf{p}| \\
 &+ \frac{1}{k_B T} \left[3B_{\text{eff}}(\phi) \cos \phi - \frac{\partial B_{\text{eff}}(\phi)}{\partial \phi} \sin \phi \right] |\mathbf{p}|^2 \\
 &+ \frac{1}{k_B T} \left[4C_{\text{eff}}(\phi) \cos \phi - \frac{\partial C_{\text{eff}}(\phi)}{\partial \phi} \sin \phi \right] |\mathbf{p}|^3 + \mathcal{O}(|\mathbf{p}|^4) \\
 Y &= Y_c^{(g)} + \frac{1}{k_B T} \left[2A_{\text{eff}}(\phi) \sin \phi + \frac{\partial A_{\text{eff}}(\phi)}{\partial \phi} \cos \phi \right] |\mathbf{p}| \\
 &+ \frac{1}{k_B T} \left[3B_{\text{eff}}(\phi) \sin \phi + \frac{\partial B_{\text{eff}}(\phi)}{\partial \phi} \cos \phi \right] |\mathbf{p}|^2 \\
 &+ \frac{1}{k_B T} \left[4C_{\text{eff}}(\phi) \sin \phi + \frac{\partial C_{\text{eff}}(\phi)}{\partial \phi} \sin \phi \right] |\mathbf{p}|^3 + \mathcal{O}(|\mathbf{p}|^4),
 \end{aligned} \tag{63}$$

where $(X_c^{(g)}, Y_c^{(g)})$ represents the 2D ECS derived from $\gamma_1(\phi)$ as follows:

$$X_c^{(g)} = \frac{\gamma_1(\phi)}{k_B T} \cos \phi - \frac{1}{k_B T} \frac{\partial \gamma_1(\phi)}{\partial \phi} \sin \phi,$$

$$Y_c^{(g)} = \frac{\gamma_1(\phi)}{k_B T} \sin \phi + \frac{1}{k_B T} \frac{\partial \gamma_1(\phi)}{\partial \phi} \cos \phi. \quad (64)$$

5.4.1. $T \leq T_{f,2}$ In the case of the first-order shape transition on the ECS, the surface of the minimum Andreev surface free energy is realized with respect to (X, Y) . From the definition of $\tilde{f}(X, Y)$ together with Eq. (64), we have

$$\begin{aligned} \tilde{f}_{\text{eff}}(X, Y)/k_B T &= Z_{\text{eff}}(X, Y) = f_{\text{eff}}(\mathbf{p})/k_B T - X p_x - Y p_y \\ &= f(0)/k_B T - A_{\text{eff}}(\phi)|\mathbf{p}|^2 - 2B_{\text{eff}}(\phi)|\mathbf{p}|^3 - 3C_{\text{eff}}(\phi)|\mathbf{p}|^4 + \mathcal{O}(|\mathbf{p}|^5). \end{aligned} \quad (65)$$

When $T < T_{f,2}$ and $\phi = \pi/4$, we have obtained $n_0^{(1)} > 0$ in §4.3 and $\gamma_1^{(1)} < 0$ in §3.4, then we have $A_{\text{eff}}(\pi/4) < 0$. Accordingly, the first-order shape transition occurs at the facet edge of (001) facet.

While, for (111) surface, Andreev surface free energy becomes

$$\begin{aligned} \tilde{f}(111)/k_B T &= Z_{(111)}(X_{(111)}, Y_{(111)}) \\ &= f(1, 1)/k_B T - X_{(111)} - Y_{(111)}, \end{aligned} \quad (66)$$

where $(X_{(111)}, Y_{(111)})$ is the coordinates on the (111) surface. If $Z_{(111)}(X, Y) < Z_{\text{eff}}(X, Y)$, the surface $Z = Z_{\text{eff}}(X, Y)$ is truncated by the plane $Z = Z_{(111)}(X, Y)$, since the Andreev surface free energy of (111) surface is smaller than that of curved area. The expression of the line of intersection between (001) surface and (111) surface is obtained from $Z_{\text{eff}}(X_c^{(i)}, Y_c^{(i)}) = Z_{(111)}(X_c^{(i)}, Y_c^{(i)})$ like

$$Y_c^{(i)} = -X_c^{(i)} + f(1, 1)/k_B T - f(0)/k_B T. \quad (67)$$

When $(X_c^{(i)}, Y_c^{(i)})$ locates inside of the closed curve $(X_c^{(g)}, Y_c^{(g)})$, the EFS is expressed by the curve $(X_c^{(g)}, Y_c^{(g)})$ truncated by the line $(X_c^{(i)}, Y_c^{(i)})$. The ECS for $T < T_{f,2}$ is just the case, which is consistent with the results in §3.2.

5.4.2. $T_{f,2} < T \leq T_{f,1}$ For the temperature $T_{f,2} < T \leq T_{f,1}$, the non-universal behavior on the ECS obtained by the PWFRG calculation is understood as the quasi non-universal behavior on the ECS, where ‘‘quasi’’ means the $f_{\text{eff}}(\mathbf{p})$ is obtained from the $f_n(\rho_n)$ of the GMPT universal type. In the temperature region, $(X_c^{(i)}, Y_c^{(i)})$ locates outside of the closed curve $(X_c^{(g)}, Y_c^{(g)})$. Hence, $(X_c^{(g)}, Y_c^{(g)})$ gives the facet contour of the (001) facet. Shape exponents are obtained by studying the profile of the ECS expressed by Eq. (63). In the case of $\phi = \pi/4$ and if we choose the axes so that we have $X = Y$, we obtain $\partial A_{\text{eff}}/\partial \phi = \partial B_{\text{eff}}/\partial \phi = \partial C_{\text{eff}}/\partial \phi = 0$ from Eq. (63). Consequently, we have expression for $r = \sqrt{2}(X - X_c^{(g)}) = \sqrt{2}(Y - Y_c^{(g)})$ as follows:

$$k_B T r = 2A_{\text{eff}}(\pi/4)p_r + 3B_{\text{eff}}(\pi/4)p_r^2 + 4C_{\text{eff}}(\pi/4)p_r^3 + \mathcal{O}(p_r^4), \quad (68)$$

where $p_r = |\mathbf{p}| = \sqrt{2}p_x = \sqrt{2}p_y$ defined in Eq. (10). In the temperature region, $0 < n_0^{(1)}$ in §4.3 and $0 \leq \gamma_1^{(1)}(\pi/4)$ in §3.4, then we have $A_{\text{eff}}(\pi/4) \geq 0$.

Let us define $p_{r\pm}^*$ so that $\partial r(p_r)/\partial p_r = 0$. We have

$$p_{r\pm}^* = \frac{1}{12C_{\text{eff}}} \left[-3B_{\text{eff}} \pm \sqrt{9B_{\text{eff}}^2 - 24A_{\text{eff}}C_{\text{eff}}} \right]. \quad (69)$$

Here, we abbreviate the notation with respect to the angle ϕ . In the region $p_1 < p < p_{r-}^*$ (and $p_{r+}^* < p < p_0$ if exists), the vicinal surface with the regular train of steps becomes metastable state. And in the region $p_{r-} < p < p_0$ (or $p_{r-} < p < p_{r+}$), the vicinal surface with the regular train of steps becomes thermodynamically unstable.

Let us discuss the shape exponents and the ‘‘amplitude’’ of the surface slope. By comparing the form of vicinal surface free energies Eq. (44) with Eq. (48), we regard $\zeta = 2$ in Eq. (48). From Eq. (54)-Eq. (56), we have

$$\theta_n = 2, \quad \theta_t = 2\theta_n = 4, \quad (70)$$

$$p_r = \frac{k_B T}{2A_{\text{eff}}} r, \quad p_t = \frac{(k_B T)^3}{4A_{\text{eff}} \tilde{\gamma}_1^2} |t|^3 \quad (r, |t| \rightarrow 0). \quad (71)$$

The shape exponents obtained from Fig. 11 calculated by the PWFRG method in §3.3 are consistent with the ones in Eq. (70) within errors.

While, the Gaussian curvature obtained from Eq. (62) with $\zeta = 2$ becomes $K = 0$ at the facet edge ($p = 0$) of (001) facet with $\phi = \pi/4$. Hence, for $\phi = \pi/4$, the Gaussian curvature jump at the facet contour like the universal case does not occur.

We estimate the value of $A_{\text{eff}}/k_B T$ at $k_B T/\epsilon = 0.36$ from p_r calculated by the PWFRG method (A_1 for the broken line in Fig. 12 (a)), and obtain as $A_{\text{eff}}/k_B T = (6.22 \pm 0.06) \times 10^{-3}$. Using this value of $A_{\text{eff}}/k_B T$ and the value of $\mathcal{A}_t(\pi/4)$ calculated by the PWFRG method, $\tilde{\gamma}_1/k_B T$ is obtained as $\tilde{\gamma}_1/k_B T = 1.39 \pm 0.03$ from Eq. (71). The value of $\tilde{\gamma}_1/k_B T$ agrees well with $\tilde{\gamma}(\pi/4)_{\text{Ising}}/k_B T$ (Eq. (21)). Consequently, in the $p_r \rightarrow 0$ limit, step-droplets ‘‘evaporate’’ to single steps. We also have $\gamma_1^{(1)}/k_B T = (2.75 \pm 0.05) \times 10^{-3}$ from the value of $A_{\text{eff}}/k_B T$ and the value of $n_0^{(1)} = 2.26$ obtained in Fig. 18. The smallness of $\gamma_1^{(1)}/k_B T$ is consistent with the experimental observation on Si(113)[92].

5.4.3. $T_{f,1} < T$ From the results in §4.3, the vicinal surface with $p_r < p_r^{(c)}$ shows GMPT universal behavior of the single step, where $p_r^{(c)}$ has the value of ~ 0.02 at $k_B T/\epsilon = 0.37$ (Fig. 11). In the limit of $p_r \rightarrow 0$, $\gamma_1^{(1)}/k_B T$ is considered to become zero, and then $A_{\text{eff}}(\pi/4) = 0$. The effective vicinal surface free energy (Eq. (44)) restores the GMPT universal form. Regarding ζ as $\zeta = 3$ in Eq. (48), we have from Eq. (54)-Eq. (56),

$$\theta_n = 3/2, \quad \theta_t = 2\theta_n = 3, \quad (72)$$

$$p_x = p_r/\sqrt{2} = \sqrt{\frac{k_B T}{6B_{\text{eff}}(\pi/4)}} r^{1/2},$$

$$|p_x - p_y| = \sqrt{2} p_t = \frac{(k_B T)^2}{\sqrt{3B_{\text{eff}}(\pi/4)\tilde{\gamma}_1(\pi/4)^3}} |t|^2. \quad (73)$$

From p_r calculated by the PWFRG method, we have $B_{\text{eff}}(\pi/4)/k_B T = 0.281 \pm 0.008$. While $B_1(\pi/4)/k_B T$ at $k_B T/\epsilon = 0.37$ estimated by use of the step stiffness of the Ising model (Eq. (21)) with universal relationship (Eq. (23)) amounts to $B_1(\pi/4)/k_B T = 1.206$. Then, from Eq. (46), we have $\gamma_1^{(2)}(\pi/4)/k_B T = -0.64 \pm 0.08$, where we used $n_0^{(1)} = 1.45$ (Fig. 18) and $\gamma_1^{(1)}(\pi/4) = 0$.

6. Summary

The restricted solid-on-solid (RSOS) model with the inter-ledge attraction of the point contact type (p-RSOS model)[31, 32] is presented to study the vicinal surface with microscopic local step attractions (Eq. (2)). The microscopic inter-ledge bonds are formed locally at the collision points between adjacent steps, where ϵ is the microscopic ledge energy, ϵ_{int} is the microscopic inter-ledge interaction energy. In the model, no long range interactions such as elastic interaction are contained.

The surface gradients $\mathbf{p} = (p_x, p_y) = (\partial z/\partial x, \partial z/\partial y)$ and the Andreev surface free energy $\tilde{f}(\boldsymbol{\eta})$ [40] of the p-RSOS model with $\epsilon_{\text{int}}/\epsilon = -0.5$ are calculated statistically as the function of the Andreev field $\boldsymbol{\eta}$ (§3). For the calculations, we adopt the transfer matrix method. We use the product wave-function renormalization group (PWFRG) algorithm[75, 81] for the efficient diagonalization of the transfer matrix.

Step-droplets in the vicinal surface of the p-RSOS model with $\epsilon_{\text{int}}/\epsilon = -0.5$ in the equilibrium are demonstrated by Monte Carlo method with Metropolis algorithm (§4.3). The simulated surface is tilted relative to (001) surface along $\langle 110 \rangle$ direction ($\phi = \pi/4$). The slope dependence of the mean step-height $\langle n \rangle$ is calculated by the Monte Carlo method.

In order to study the shape transition on the equilibrium shape $z(x, y)$ of the crystal particulate (the equilibrium crystal shape, ECS)[40] in detail, we introduce the reduced ECS $Z(X, Y)$ such that $X = \eta_x/k_B T = -\lambda x$, $Y = \eta_y/k_B T = -\lambda y$, and $Z = \tilde{f}(X, Y)/k_B T$. Here, λ is the Lagrange multiplier relating to the volume of the particulate. We analyze the reduced ECS calculated by use of PWFRG method for several temperatures. Then, we obtain the first-order shape transition around (111) facet (§3.1). There are two characteristic temperatures, $T_{f,1}$ and $T_{f,2}$. For $T < T_{f,1}$, where $k_B T_{f,1}/\epsilon = 0.3610 \pm 0.0005$, first-order shape transition occurs around (111) facet. For $T < T_{f,2}$, where $k_B T_{f,2}/\epsilon = 0.3585 \pm 0.0007$, (001) facet directly contacts (111) facet with the line of intersection between (001) surface and (111) surface. For $T_{f,1} < T$, the first-order shape transition does not occur around (001) facet nor around (111) facet.

In the temperature region $T_{f,2} < T < T_{f,1}$ with $\phi = \pi/4$, the first-order shape transition is obtained by the PWFRG calculations around (111) facet. In the case of $k_B T/\epsilon = 0.36$, p_x ($= p_y = p_r/\sqrt{2}$) jumps from $p_1 = 0.349 \pm 0.002$ to $p_0 = 1$ ($=$ (111) surface) at $X = Y = X_q = 2.084$ ($> X_c = Y_c = 2.0808 \pm 0.0002$). While near (001) facet edge, non-universal shape exponents and non-universal step interaction coefficient $B(\phi)$ are obtained from the PWFRG calculation. We describe the ECS around (001) facet as $|Z(r) - Z_c| = \mathcal{A}_n(\pi/4)r^{\theta_n}$ (§3.3) along the line r normal to the facet contour, and $|Z(t) - Z_c| = \mathcal{A}_t(\pi/4)|t|^{\theta_t}$ along the line t tangent to the facet contour, where Z_c the height level of the (001) facet, θ_n the normal shape exponent, $\mathcal{A}_n(\pi/4)$ the normal amplitude, θ_t the tangential shape exponent, and $\mathcal{A}_t(\pi/4)$ the tangential amplitude. At $k_B T/\epsilon = 0.36$, we have obtained $\theta_n = 1.98 \pm 0.03$, $\mathcal{A}_n(\pi/4) = 40.61 \pm 0.02$, $\theta_t = 3.92 \pm 0.10$, and $\mathcal{A}_t(\pi/4) = 7.2 \pm 1.0$ by use of PWFRG calculations.

We consider that the formation of step-droplets causes the non-universal behaviors

on the profile of the ECS. We derive the effective vicinal surface free energy $f_{\text{eff}}(\mathbf{p})$ (§5.1) from the vicinal surface free energy of the bunched step of the Gruber-Mullins-Pokrovsky-Talapov (GMPT) universal type $f_n(\rho_n)$, where n the height of the bunched step, and ρ_n the step density of the bunched step. In order to derive $f_{\text{eff}}(\mathbf{p})$, we take into account the slope dependence on the mean step-height of the step-droplet (§4.3). The effective vicinal surface free energy has the form such as $f_{\text{eff}}(\mathbf{p}) = f(0) + \gamma_1(\phi)|\mathbf{p}| + A_{\text{eff}}(\phi)|\mathbf{p}|^2 + B_{\text{eff}}(\phi)|\mathbf{p}|^3 + C_{\text{eff}}(\phi)|\mathbf{p}|^4 + \mathcal{O}(|\mathbf{p}|^5)$ (Eq. (44), §5.1). In the form, the quadratic term $A_{\text{eff}}(\phi)|\mathbf{p}|^2$ appears. $A_{\text{eff}}(\phi)$ consists of $n_0^{(1)}(\phi)$ and $\gamma_1^{(1)}(\phi)$ (Eq. (45)). Further, we derive expressions for the shape exponents (θ_n and θ_t) and the ‘‘amplitudes’’ ($\mathcal{A}_n(\phi)$ and $\mathcal{A}_t(\phi)$) as shown in Eq. (54)-(56) (§5.2) for general ζ in the extended vicinal surface free energy such that $f_\zeta(\mathbf{p}) = f(0) + \gamma(\phi)|\mathbf{p}| + B_\zeta(\phi)|\mathbf{p}|^\zeta + \mathcal{O}(|\mathbf{p}|^{\zeta+1})$.

Using $f_{\text{eff}}(\mathbf{p})$ with the general expressions of the shape exponents and the amplitudes at $k_B T/\epsilon = 0.36$, we obtain $\theta_n = 2$, $\theta_t = 4$, $A_{\text{eff}}(\pi/4)/k_B T = (6.22 \pm 0.06) \times 10^{-3}$, $n_0^{(1)}(\pi/4) = 2.26 \pm 0.08$, and $\gamma_1^{(1)}(\pi/4)/k_B T = (2.75 \pm 0.05) \times 10^{-3}$ (§5.4). We also have reproduced $\tilde{\gamma}_1(\phi)$ from Eq. (56) in $r, |t| \rightarrow 0$ limit, and the obtained value agrees with the $\tilde{\gamma}(\pi/4)_{\text{Ising}}$. This means that the step-droplets evaporate to the steps of the unit height in the limit of $|\mathbf{p}| \rightarrow 0$ (§5.4.2).

For $T_{f,1} \lesssim T$, in the PWFRG results, the normal shape exponent θ_n crosses over from ~ 2 to 1.5 as $|\mathbf{p}|$ decreases. In the limit of $p_x \rightarrow 0$, we have $\theta_n = 1.5$, $\mathcal{A}_n(\pi/4) = 0.73 \pm 0.04$, $\theta_t = 2.8 \pm 0.3$, and $\mathcal{A}_t(\pi/4) = 0.062 \pm 0.018$ (§3.3, §3.4). In this case, $A_{\text{eff}} = 0$ for $|\mathbf{p}| \rightarrow 0$, since $\gamma_1^{(1)} = 0$. Hence, $f_{\text{eff}}(\mathbf{p})$ recovers the GMPT universal form. The universal relationship between the step interaction coefficient $B_{\text{eff}}(\pi/4)$ and $\tilde{\gamma}_1(\pi/4)$ [52] (Eq. (23)), however, is unsatisfied, since $B_{\text{eff}}(\phi)$ in $f_{\text{eff}}(\mathbf{p})$ is described as $B_{\text{eff}}(\phi) = (1/2)[n_0^{(2)}(\phi)\gamma_1^{(1)}(\phi) + n_0^{(1)}(\phi)\gamma_1^{(2)}(\phi)] + B_1(\phi)$ (§5.1). Comparing the normal amplitude and the tangential amplitude obtained by PWFRG calculations with the ones obtained by $f_{\text{eff}}(\mathbf{p})$, at $k_B T/\epsilon = 0.37$, we obtain $n_0^{(1)} = 1.45$, $\gamma_1^{(1)}(\phi) = 0$, $B_{\text{eff}}(\pi/4)/B(\pi/4)_{\text{Ising}} = 0.233$, and $\gamma_1^{(2)}(\pi/4)/k_B T = -0.64 \pm 0.08$ (§5.4).

For $T < T_{f,2}$, well developed step-droplets are formed like step faceting. The step-droplets are demonstrated by the Monte Carlo simulation with the simple Metropolis algorithm near equilibrium.

From the zeros of \mathbf{p} in the PWFRG calculations, we obtain the equilibrium facet shape (EFS) of (001) facet at $k_B T/\epsilon = 0.3$. The EFS agrees with the two-dimensional (2D) ECS of the nn square Ising model except for the truncated part cut by the line of intersection between (001) surface and (111) surface (§3.2). The step tension of the step-height n for the bunched step is approximated by $\gamma_n(\phi) \approx \sqrt{2}(\epsilon + \epsilon_{\text{int}}/2) \times n$, for $\phi = \pi/4$. Hence, in the temperature range, we have $\gamma_1^{(1)}(\pi/4) < 0$, which leads $A_{\text{eff}} < 0$.

7. Conclusion

For $T < T_{f,2}$, (001) facet on the ECS of p-RSOS model directly contacts with (111) facet. For $T_{f,2} < T \lesssim T_{f,1}$, the shape exponents near (001) facet edge with $\phi = \pi/4$ has quasi non-universal values such as the shape exponent along the normal line $\theta_n = 2$,

and the shape exponent along the tangential line $\theta_t = 4$ due to the formation of the step-droplets. In the $|\mathbf{p}| \rightarrow 0$ limit, the step-droplets “evaporate” to the steps with the unit height, and the step tension and the step stiffness converges to $\gamma_1(\pi/4)$ and $\tilde{\gamma}_1(\pi/4)$, respectively. For $T_{f,1} \lesssim T$, the shape exponents near (001) facet edge have the GMPT universal values. The effective step interaction coefficient $B_{\text{eff}}(\pi/4)$, however, does not satisfy the universal relationship between $B_{\text{eff}}(\pi/4)$ and $\tilde{\gamma}_1(\pi/4)$. The quasi non-universal behaviors obtained by the PWFRG calculations are reproduced from the effective vicinal surface free energy $f_{\text{eff}}(\mathbf{p})$, where the slope dependence on the mean step-height of the step-droplet are taken into account, with using the general expressions on the shape exponents and the amplitudes.

8. Acknowledgements

Author thanks to Prof. T. Yamamoto and Prof. K. Sudoh for discussions. This work was partially supported by the “Research for the Future” Program from The Japan Society for the Promotion of Science (JSPS-RFTF97P00201) and by the Grant-in-Aid for Scientific Research from Ministry of Education, Science, Sports and Culture (No.09640462 and No. 15540323).

References

- [1] W. W. Mullins, *Philos. Mag.* **6**, 1313 (1961). N. Cabrera, *Symposium on Properties of Surfaces*, p24 (Americal Society for Testing and Materials, Philadelphia 1963).
- [2] S. Stoyanov, *Jpn. J. Appl. Phys.* **30**, 1 (1991). A. V. Latyshev, A. L. Aseev, A. B. Krasilnikov and S. I. Stenin, *Surf. Sci.* **213**, 157 (1989).
- [3] A. Natori, *Jpn. J. Appl. Phys.* **33**, 3538 (1994).
- [4] M. Sato, M. Uwaha and Y. Saito, *Phys. Rev. B* **62**, 8452 (2000).
- [5] A. Pimpinelli and J. Villain, *Physics of Crystal Growth*, (Cambridge University Press, 1998).
- [6] D. Kandel and J. D. Weeks, *Phys. Rev. Lett.* **74**, 3632 (1995).
- [7] D. Kandel and J. D. Weeks, *Phys. Rev. B* **49**, 5554 (1994); *ibid* **B52**, 2154 (1995).
- [8] J. Krug, *Europhys. Lett.* **60**, 778 (2002).
- [9] F. C. Frank, *Growth and Perfection of Crystals*, ed. R. H. Doremus et al., 411 (1958). F. C. Frank, *Metal Surfaces*, 1 ASM (1963).
- [10] C. Teichert, *Phys. Rep.* **365**, 335 (2002).
- [11] V. B. Shenoy, S. Zhang, and W. F. Saam, *Phys. Rev. Lett.* **81**, 3475-3478 (1998); *Surf. Sci.* **467**, 58 (2000).
- [12] M. Lassig, *Phys. Rev. Lett.* **77**, 526 (1996).
- [13] S. Song and G. J. Mocherie, *Phys. Rev. Lett.* **73**, 995 (1994); *Phys. Rev. B* **51**, 10068 (1995).
- [14] S. M. Bhattacharjee, *Phys. Rev. Lett.* **76**, 4568 (1996).
- [15] T. L. Einstein, H. L. Richards, S. D. Cohen, O. Pierre-Louis, M. Giesen, *Appl. Surf. Sci.* **175-176**, 62 (2001).
- [16] H. Ibach and W. Shmickler, *Phys. Rev. Lett.* **91**, 016106 (2003); *Surf. Sci.* **573**, 24 (2004).
- [17] N. C. Bartelt, T. L. Einstein and E. D. Williams, *Surf. Sci.* **276**, 308 (1992).
- [18] R. J. Phaneuef, N. C. Bartelt, E. D. Williams, W. Swiech, and E. Bauer, *Phys. Rev. Lett.* **71**, 2284 (1993).
- [19] H. -C. Jeong and J. D. Weeks, *Phys. Rev. Lett.* **75**, 4456 (1995).
- [20] T. Ogino, H. Hibino, and Y. Homma, *Crit. Rev. Solid State and Mater. Sci.* **24**, 227 (1999).

- [21] N. Akutsu, Y. Akutsu and T. Yamamoto, *Prog. Theor. Phys.* **105**, 361 (2001).
- [22] M. Horn-von Hoegen, H. Minoda, K. Yagi, F. Meyer zu Heringdorf, and D. Kähler, *Th. Schmidt, Surf. Sci.* **402-404**, 464 (1998); M.Horn-von Hoegen, F. -J. Meyer zu Heringdorf, D. Kähler, Th. Schmidt and E. Bauer, *Thin solid Films* **336**, 16 (1998). H. Minoda, K. Yagi, F. -J. Meyer zu Heringdorf, A. Meier, D. Kähler, and M. Horn-von Hoegen, *Phys. Rev.* **B59**, 2363 (1999).
- [23] H. Minoda and K. Yagi, *Phys. Rev.* **B60**, 2715 (1999).
- [24] M. Aono, Y. Fukui, T. Urano, K. Ojima, and M. Yoshimura, *Surf. Sci.* **507-510**, 417 (2002).
- [25] Y. Takahashi, H. Minoda, Y. Tanishiro, and K. Yagi, *Surf. Sci.* **433-435**, 512 (1999).
- [26] S. Fölsch, G. Meyer, K. H. Rieder, M. Horn-von Hoegen, T. Schmidt, and M. Henzler, *Surf. Sci.* **394**, 60 (1997).
- [27] N. Akutsu, Y. Akutsu and T. Yamamoto, *Surf. Sci.* **493/1-3**, 475 (2001).
- [28] N. Akutsu, Y. Akutsu and T. Yamamoto, *Phys. Rev. B* **67**, 125407 (2003); *J. Crys. Growth*, 237 (2002).
- [29] N. Akutsu and Y. Kakii, *Appl. Surf. Sci.* **254**, 7535 (2008).
- [30] N. Akutsu, H. Hibino, and T. Yamamoto, *e-J. Surf. Sci. Nanotech.* **7**, 39 (2009).
- [31] N. Akutsu, *Appl. Surf. Sci.* **256**, 1205 (2009).
- [32] N. Akutsu, *J. Cryst. Growth* **318** 10 (2011), doi:10.1016/j.jcrysgr.2010.10.088.
- [33] G. Wulff, *Z. Kristallogr.* **34**, 449 (1901).
- [34] M. von Laue, *Z. Kristallogr.* **105**, 124 (1944).
- [35] W. K. Burton, N. Cabrela and F. C. Frank, *Philos. Trans. Roy. Soc. London A* **243**, 299 (1951).
- [36] C. Herring, *Phys. Rev.* **82**, 87 (1951).
- [37] S. Toschev, *Crystal Growth, An Introduction*, ed. P. Hartman (North-Holland, 1973), 328.
- [38] J. K. MacKenzie, A. J. W. Moore and J. F. Nicholas, *J. Chem. Phys. Solids* **23**, 185 (1962).
- [39] L. D. Landau and E. M. Lifshitz, *Statistical Physics*, 2nd edition (Oxford: Pergamon, 1968).
- [40] A. F. Andreev, *Zh. Eksp. Theor. Fiz.* **80**, 2042 (1981) [*Sov. Phys. JETP* **53**, 1063 (1982)].
- [41] A. Ookawa, *Crystal Growth (Syōkabō, Tokyo, 1977)*, in Japanese.
- [42] J. C. Heyraud and J. J. Métois, *J. Cryst. Growth* **50**, 571 (1980); J. C. Heyraud and J. J. Métois, *Acta Metal.* **28**, 1789 (1980).
- [43] R. Kern, G. Le Ley and J. J. Metois, *Current Topics in Materials Science*, ed. E. Kaldis Vol. 3 (North-Holland, Amsterdam, 1979) p. 135.
R. Kern, *Morphology of Crystals*, ed. I. Sunagawa (Terra Scientific Publishing Company, Tokyo 1987).
- [44] N. Akutsu and Y. Akutsu, *J. Phys. Soc. Jpn.* **56**, 1443 (1987).
- [45] E. E. Gruber and W. W. Mullins, *J. Phys. Chem. Solids* **28** 6549 (1967). V. L. Pokrovsky and A. L. Talapov, *Phys. Rev. Lett.* **42** 65 (1979), [*Sov. Phys. JETP* **51** 134 (1980)].
- [46] F. D. M. Haldane and J. Villain, *J. de Physique* **42**, 1673 (1981).
- [47] T. Izuyama and Y. Akutsu: *J. Phys. Soc. Jpn.* **51**, 50 (1982). T. Yamamoto and T. Izuyama: *J. Phys. Soc. Jpn.* **56**, 632 (1987).
- [48] C. Jayaprakash, W. F. Saam, and S. Teitel, *Phys. Rev. Lett.* **50**, 2017 (1983).
- [49] H. J. Schultz, *J. Phys. (Paris)* **46**, 257 (1985); G. F. Gallet, P. Nozières, S. Balibar and E. Rolley, *Europhys. Lett.* **2**, 701 (1986).
- [50] H. van Beijeren and I. Nolden, *Structure and Dynamics of Surfaces*, Vol. 2, 259, Ed. W. Schommers and P. von Blancken-Hagen, (Springer-Verlag, Berlin Heidelberg, 1987).
- [51] N. Akutsu and Y. Akutsu, *J. Phys. Soc. Jpn.* **56**, 2248 (1987); M. Uwaha, unpublished.
- [52] Y. Akutsu, N. Akutsu and T. Yamamoto, *Phys. Rev. Lett.* **61**, 424 (1988). T. Yamamoto, Y. Akutsu and N. Akutsu, *J. Phys. Soc. Jpn.* **57**, 453 (1988). L. V. Mikheev and V. L. Pokrovsky, *J. de Phys. I* **1**, 373 (1991).
- [53] W. F. Saam, *Phys. Rev. Lett.* **62**, 2636 (1989).
- [54] Y. Akutsu, N. Akutsu and T. Yamamoto, *Phys. Rev. Lett.* **62**, 2637 (1989).
- [55] T. Yamamoto, Y. Akutsu and N. Akutsu, *J. Phys. Soc. Jpn.* **58**, 3531 (1989). T. Yamamoto, N. Akutsu and Y. Akutsu, *J. Phys. Soc. Jpn.* **59**, 3831 (1990). *J. Phys. Soc. Jpn.* **60**, 3600 (1991).

- [56] T. Yamamoto, Y. Akutsu and N. Akutsu, *J. Phys. Soc. Jpn.* **63**, 915 (1994).
- [57] T. Ohachi and I. Taniguchi, *J. Crystal Growth* **65**, 84 (1983); *Morphology and Growth Unit Crystals*, ed. I. Sunagawa (Terra Scientific Publishing, Tokyo, 1987).
- [58] A. V. Babkin, K. O. Keshishev, D. B. Kopeliovich and A. Ya. Parshin, *JETP Lett.* **39**, 633 (1984).
- [59] P. E. Wolf, G. F. Gallet, S. Balibar, E. Rolley and P. Nozières, *J. de Phys.* **46**, 1987 (1985).
- [60] S. Baliber and P. Noziere, *Solid State Commun.* **92**, 19 (1994).
- [61] S. Baliber, H. Alleys and A. Ya. Parshin, *Rev. Mod. Phys.* **77**, 317 (2005).
- [62] Y. Carmi, S.G. Lipson and E. Polturak, *Phys. Rev. B* **36**, 1894 (1987).
- [63] A. Pavlovska and E. Bauer, *Europhys. Lett.* **9**, 797 (1989).
- [64] J. C. Heyraud and J. J. Métois, *Surf. Sci.* **177**, 213 (1986). J. J. Métois and J. C. Heyraud, *Surf. Sci.* **180**, 647 (1987).
- [65] J. M. Bermond, J. J. Métois, X. Egea and F. Floret, *Surf. Sci.* **330**, 48 (1995). T. Suzuki, J. J. Métois and K. Yagi, *Surf. Sci.* **339**, 105 (1995). T. Suzuki, H. Minoda, Y. Tanishiro, K. Yagi, *Surface Review and Letters*, **6**, 985 (1999).
- [66] E. D. Williams, R. J. Phaneuf, J. Wei, N. C. Bartelt and T. L. Einstein, *Surf. Sci.* **294**, 219 (1993); *ibid.* *Surf. Sci.* **310**, 451 (1994).
- [67] J. J. Métois and P. Müller, *Surf. Sci.* **548**, 13 (2004). H. P. Bonzel and A. Emundts, *Phys. Rev. Lett.* **84**, 5804 (2000).
- [68] W-C. Cheng and P. Wynblatt, *Surf. Sci.* **364**, 417 (1996). K. Arenhold, S. Surnev, H. P. Bonzel and P. Wynblatt, *Surf. Sci.* **424**, 271 (1999).
- [69] M. Nowicki, C. Bombis, A. Emundts, H. P. Bonzel and P. Wynblatt, *Europhys Lett.* **59**, 239 (2002). M. Nowicki, C. Bombis, A. Emundts, H. P. Bonzel and P. Wynblatt, *New J. Phys.* **4**, 60 (2002).
- [70] N. Akutsu and Y. Akutsu, *Prog. Theor. Phys.* **116**, 983 (2006). Y. Akutsu, N. Akutsu, and T. Yamamoto, *cond-mat/9803189*, (1998).
- [71] C. Rottman and M. Wortis, *Phys. Rep.* **103**, 59 (1984); *Phys. Rev.* **B29**, 328 (1984).
- [72] C. Jayaprakash and W. F. Saam, *Phys. Rev.* **B30**, 3916 (1984).
- [73] C. Jayaprakash, C. Rottman and W. F. Saam: *Phys. Rev.* **B30**, 6549 (1984).
- [74] K. Sogo, Y. Akutsu and T. Abe, *Prog. Theor. Phys.* **70**, 739 (1983). T. T. Truong and M. den Nijs, *J. Phys.* **A19**, L645 (1986).
- [75] T. Nishino and K. Okunishi, *J. Phys. Soc. Jpn.* **64**, 4084 (1995).
- [76] Y. Hieida, K. Okunishi and Y. Akutsu, *Phys. Lett.* **A233**, 464 (1997).
- [77] K. Okunishi, Y. Hieida and Y. Akutsu, *Phys. Rev. B* **59**, 6806 (1999).
- [78] Y. Hieida, K. Okunishi and Y. Akutsu, *New J. Phys.* **1**, 7.1 (1999).
- [79] S. Östlund and S. Rommer, *Phys. Rev. Lett* **75**, 3537 (1995); *Phys. Rev. B* **55**, 2164 (1997).
- [80] Y. Natsume, K. Ogawa, and T. Suzuki, *Computational Physics III*, in Japanese (Asakura Publishing, Tokyo, 2002).
- [81] S. R. White, *Phys. Rev. Lett.* **69**, 2863 (1992). T. Nishino, *J. Phys. Soc. Jpn.* **64**, 3598 (1995).
- [82] N. Akutsu and Y. Akutsu, *Phys. Rev. B* **57**, R4233 (1998); *Surf. Sci.* **376**, 92 (1997). Y. Honda and T. Horiguchi, *Phys. Rev.* **E56**, 3920 (1997).
- [83] Y. Akutsu and N. Akutsu, *J. Phys.* **A19**, 2813 (1986).
- [84] C. Rottman and M. Wortis, *Phys. Rev.* **B24**, 6274 (1981). J. E. Avron, H. van Beijeren, L. S. Schulman and R. K. P. Zia, *J. Phys.* **A15**, L81 (1982).
- [85] Y. Akutsu and N. Akutsu, *Phys. Rev. Lett.* **64**, 1189 (1990).
- [86] N. Akutsu and Y. Akutsu, *J. Phys. Soc. Jpn.* **59**, 3041 (1990).
- [87] M. Holzer, *Phys. Rev. Lett.* **64**, 653 (1990); *Phys. Rev.* **B42**, 10570 (1990).
- [88] N. Akutsu, *J. Phys. Soc. Jpn.* **61**, 477 (1992).
- [89] N. Akutsu and Y. Akutsu, *Surf. Sci.* **376**, 92 (1997).
- [90] N. Akutsu and Y. Akutsu, *J. Phys.: Condens. Matter*, **11**, 6653 (1999).
- [91] E. Kreyszig, *Introduction to Differential Geometry and Riemannian Geometry* (University of

Tronto Press, 1968).

- [92] K. Sudoh, T. Yoshinobu, H. Iwasaki, and E. D. Williams, Phys. Rev. Lett. **80**, 5152 (1998).